# 12. Turbomachinery

Meinhard T. Schobeiri



The following chapter consists of two sections. Section 12.1 presents a concise treatment of the theory of turbomchinery stages including the energy transfer in absolute and relative systems. Contrary to the traditional approach that treats turbine and compressor stages of axial, radial or mixed configurations differently, these components are treated from a unifying point of view.

Section 12.2 is dedicated to steady and unsteady performance of gas turbine engines, where the components are treated as generic modules. Thus, any arbitrary power generation or aircraft gas turbine engine with single or multiple shafts can be composed of these modules. Several examples show, how different gas turbine configurations can be constructed and dynamically simulated. Finally, a section about the new generation gas turbines shows, how the efficiency of gas turbines can be improved far beyond the existing level.

This chapter is based on [12.1], where the reader finds detailed explanation of relevant aerodynamic aspects of turbomachines, their component losses and efficiencies, and the design and off-design performance calculations.



## 12.1 Theory of Turbomachinery Stages

### 12.1.1 Energy Transfer in Turbomachinery Stages

Energy transfer in turbomachinery is established by means of a number of stages. A *turbomachinery stage* consists of a row of fixed, guide vanes called *stator blades*, and a row of rotating blades termed the *rotor*. To elevate the total pressure of a working fluid, *compressor stages* that partially convert the mechanical energy into potential energy are used. According to the law of conservation of energy, this energy increase requires

an external energy input which must be added to the system in the form of mechanical energy. Figure 12.1 shows a schematic of an axial compressor stage that consists of one stator and two rotor rows. In general, a *compressor component* starts with a rotor row followed by a stator row. Compressor configurations that start with an *inlet guide vane* are also found. To define a unified station nomenclature for the compressor and turbine stages, we identify station number 1 as the inlet of the stator, followed by station 2 as the rotor inlet, and station 3 as the rotor exit. The absolute and relative flow angles are counted counterclockwise from a horizontal line. This convention allows an easier calculation of the off-design behavior of compressor and turbine stages during a transient operation, as we will see later. Different angle conventions are used in the literature [12.2–5]. The working fluid enters the first rotor with an *absolute velocity* in the axial direction (Fig. 12.1b), where it is deflected in the direction of the rotor's leading edge. As a result of the rotational motion of the rotor, a major part of the mechanical energy input is converted into the potential energy of the working medium, causing the total pressure to rise. During the compression process, the absolute velocity within the stator and the relative velocity vector within the rotor decrease. To convert the total energy of a working medium into mechanical energy, *turbine stages* are used. Figure 12.2 exhibits a turbine stage within a multistage environment. As shown, the mean diameter may change from inlet to exit. The continuous increase in flow path cross section is due to the continuity requirement.

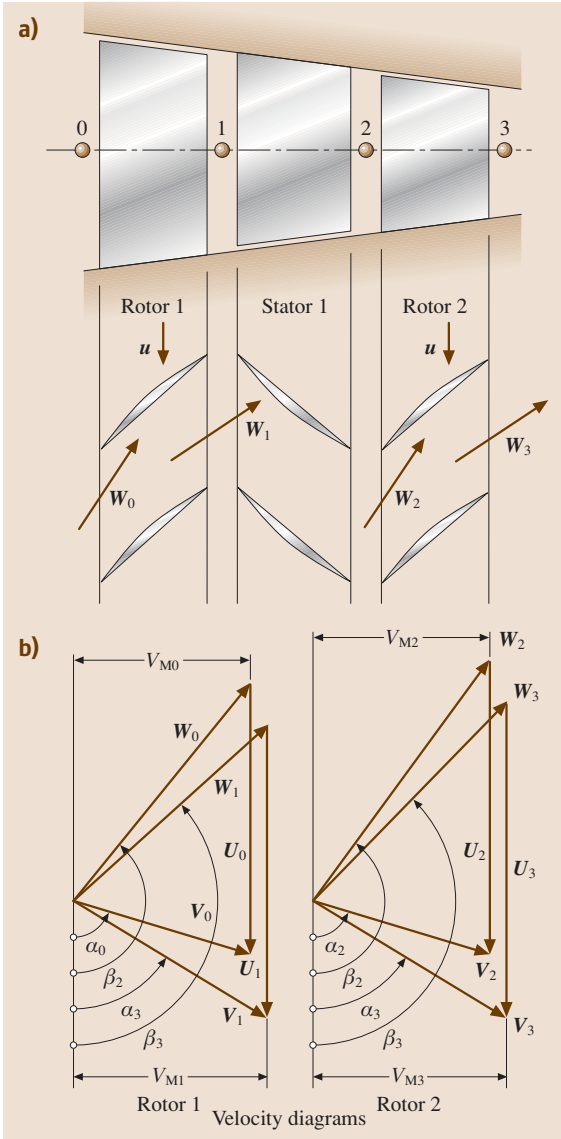


**Fig. 12.1** **(a)** An axial compressor stage with a rotor–stator–rotor configuration and **(b)** velocity diagrams for the first and second rotor

## 12.1.2 Energy Transfer in Relative Systems

Since the rotor operates in a relative frame of reference (relative system), the energy conversion mechanism is quite different from that of a stator (absolute system). A fluid particle that moves with a relative velocity $\boldsymbol{W}$ within the relative system that rotates with the angular velocity $\boldsymbol{\omega}$, has an absolute velocity

$$\boldsymbol{V} = \boldsymbol{W} + \boldsymbol{\omega} \times \boldsymbol{R} = \boldsymbol{W} + \boldsymbol{U}, \quad \boldsymbol{\omega} \times \boldsymbol{R} = \boldsymbol{U}\,, \tag{12.1}$$

where $\boldsymbol{R}$ is the radius vector of the particle in the relative system. Introducing the absolute velocity vector $\boldsymbol{V}$ in the equation of motion [12.1, Chap. 3, Eq. (3.37)] and multiplying the results with a relative differential displacement $\mathrm{d}R$, we get the energy equation for an adiabatic steady flow within a relative system

$$\mathrm{d}\left(h + \frac{1}{2}W^2 - \frac{\omega^2 R^2}{2} + gz\right) = 0 \tag{12.2}$$

or the relative total enthalpy

$$H_\mathrm{r} = h + \frac{1}{2}W^2 - \frac{\omega^2 R^2}{2} + gz = \text{const}\,. \tag{12.3}$$

Neglecting the gravitational term, $gz \approx 0$, (12.3) can be written as

$$h_1 + \frac{1}{2}W_1^2 - \frac{1}{2}U_1^2 = h_2 + \frac{1}{2}W_2^2 - \frac{1}{2}U_2^2\,. \tag{12.4}$$

Equation (12.4) is the equation for the energy transformed in a relative system. As can be seen, the transformation of kinetic energy undergoes a change while the transformation of static enthalpy is frame indifferent. With these equations together with the energy balance [12.6] we can analyze the energy transfer within an arbitrary turbine or compressor stage.

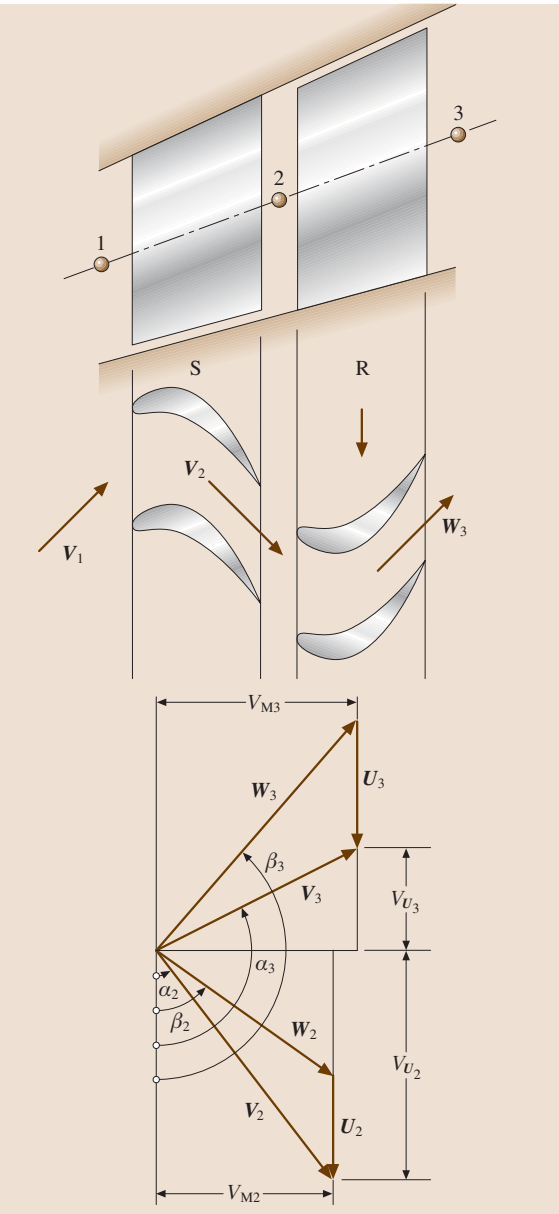


**Fig. 12.2** An axial turbine stage with velocity diagram

### 12.1.3 General Treatment of Turbine and Compressor Stages

In this chapter, compressor and turbine stages are treated from a unified physical point of view. Figures 12.3 and 12.4 show the decomposition of a turbine and a compressor stage into their stator and rotor rows. The primes $'$ and $''$ refer to stator and rotor rows, respectively. As seen, the difference between the isentropic and the polytropic enthalpy difference is expressed in terms of dissipation $\Delta h'_\mathrm{d} = \Delta h'_\mathrm{s} - \Delta h'$ for turbines and $\Delta h'_\mathrm{d} = \Delta h' - \Delta h'_\mathrm{s}$ for compressors. For the stator, the energy balance requires that $H_2 = H_1$. This leads to

$$h_1 - h_2 = \Delta h' = \frac{1}{2}\left(V_2^2 - V_1^2\right) . \tag{12.5}$$

Moving to the relative frame of reference, the relative total enthalpy $H_{\mathrm{r}2} = H_{\mathrm{r}3}$ remains constant. Thus, the energy equation for the rotor is according to (12.4) (Fig. 12.4)

$$h_2 - h_3 = \Delta h'' = \frac{1}{2}\left(W_3^2 - W_2^2 + U_2^2 - U_3^2\right) . \tag{12.6}$$

The stage specific mechanical energy balance requires (Fig. 12.5)

$$\begin{aligned} l_\mathrm{m} &= H_1 - H_3 \\ &= (h_1 - h_2) - (h_3 - h_2) + \frac{1}{2}\left(V_1^2 - V_3^2\right) . \end{aligned} \tag{12.7}$$

Inserting (12.5) and (12.6) into (12.7) yields

$$l_\mathrm{m} = \frac{1}{2}\left[\left(V_2^2 - V_3^2\right) + \left(W_3^2 - W_2^2\right) + \left(U_2^2 - U_3^2\right)\right] . \tag{12.8}$$

Equation (12.8), known as the *Euler turbine equation*, indicates that the stage work can be expressed simply in terms of absolute, relative, and rotational kinetic energies. This equation is equally applicable to turbine stages that *generate* shaft power and to compressor stages that *consume* shaft power. In the case of a turbine stage, the sign of the specific mechanical energy $l_\mathrm{m}$ is negative, which indicates that energy is removed from the system (power generation). In compressor cases, it is positive because energy is added to the system (power consumption). Before proceeding with velocity diagrams, it is of interest to evaluate the individual kinetic energy differences in (12.8). If we wish to design a turbine or a compressor stage with a high specific mechanical energy $l_\mathrm{m}$ for a particular rotational speed, then

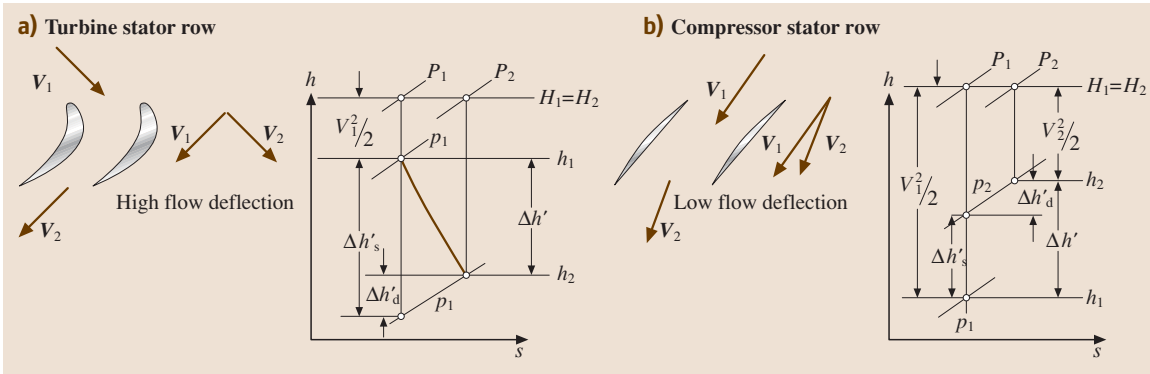


**Fig. 12.3a,b** Expansion and compression process through a turbine (**a**) and a compressor (**b**) stator row

we have two options:

1. We increase the *flow deflection*, which leads to an increase in $\left(V_2^2 - V_3^2\right)$.
2. We increase the radial difference that leads to a larger $\left(U_2^2 - U_3^2\right)$.

While option 1 is used in axial stages, option 2 is primarily applied to radial stages. These quantities are the characteristics of a stage velocity diagram at the corresponding radial section.

Using the trigonometric relation with the *angle convention* from the velocity diagram in Figs. 12.5 and 12.6, we determine the velocity components and vector relations from

$$
\begin{aligned}
&V_{m2} = W_{m2}\,, \quad V_{m3} = W_{m3}\,,\\
&\boldsymbol{W}_2 = e_1(V_{u2} - U_2) + e_2 V_{m2}\,,\\
&\boldsymbol{W}_3 = -e_1(V_{u3} - U_3) + e_2 V_{m3}\,.
\end{aligned}
\tag{12.9}
$$

In (12.9) $V_m$, $W_m$ and $V_u$, $W_u$ are the meridional and circumferential components of the absolute and relative velocities, respectively. The corresponding kinetic energy contributions are determined from

$$
\begin{aligned}
W_2^2 &= \left(V_{u2}^2 + V_{m2}^2\right) + U_2^2 - 2V_{u2}U_2\\
&= V_2^2 + U_2^2 - 2V_{u2}U_2\,,\\
W_3^2 &= V_{u3}^2 + U_3^2 + 2V_{u3}U_3 + V_{m3}^2\,,\\
W_3^2 &= V_3^2 + U_3^2 + 2V_{u3}U_3\,.
\end{aligned}
\tag{12.10}
$$

Incorporating (12.9) and (12.10) into (12.8) yields the *stage specific* work

$$
l_m = U_2 V_{u2} + U_3 V_{u3}\,. \tag{12.11}
$$

Equation (12.11) is valid for axial, radial, and mixed flow turbines and compressors. A similar relation is obtained from the scalar product of moment of momentum and the angular velocity. In conjunction with the equation of moment of momentum, one finds in the

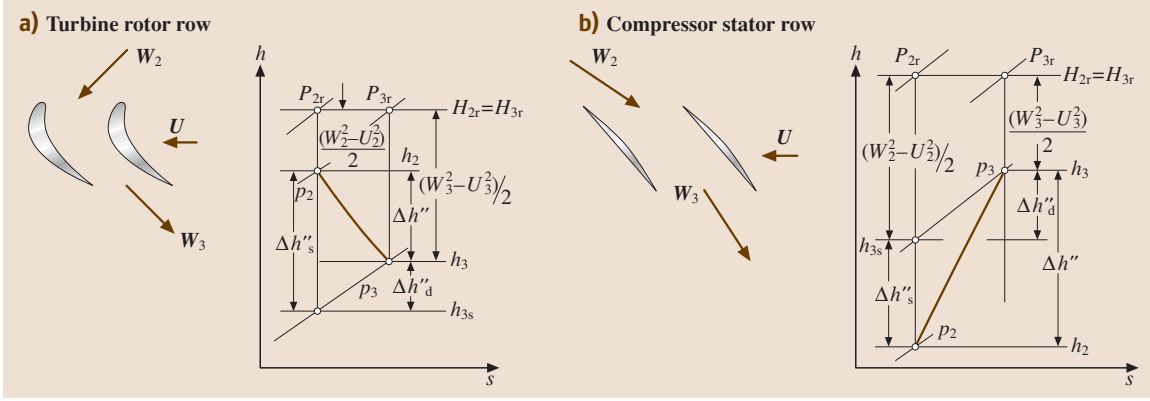


**Fig. 12.4a,b** Expansion and compression process through a turbine (**a**) and a compressor (**b**) rotor row

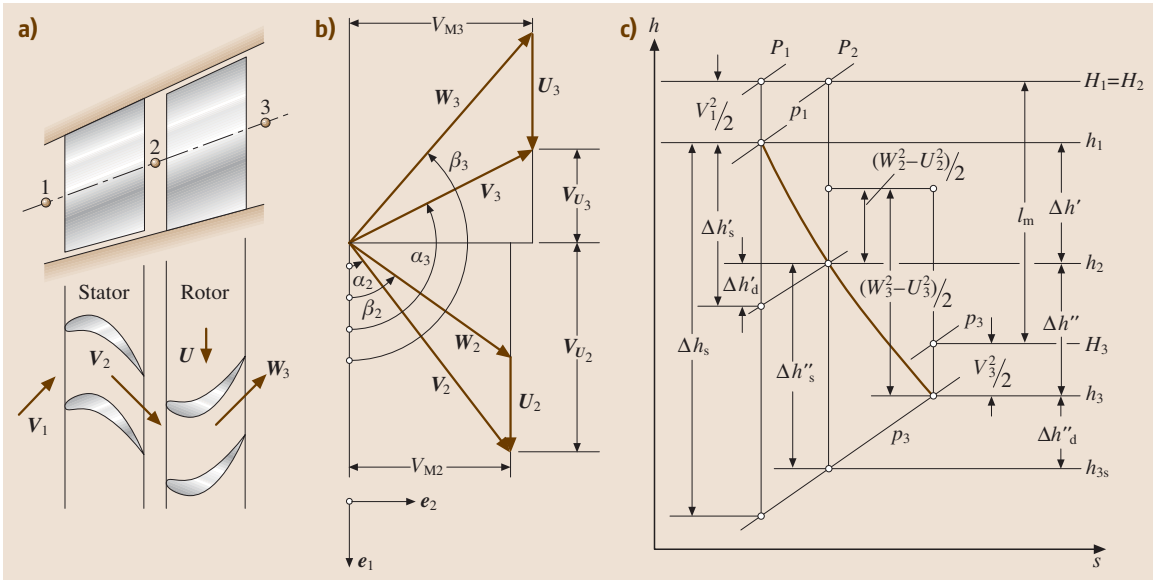


**Fig. 12.5a–c** A compressor stage (a) with the velocity diagram (b) and the expansion process (c). The direction of the unit vector $\boldsymbol{e}_1$ is identical with the rotational direction

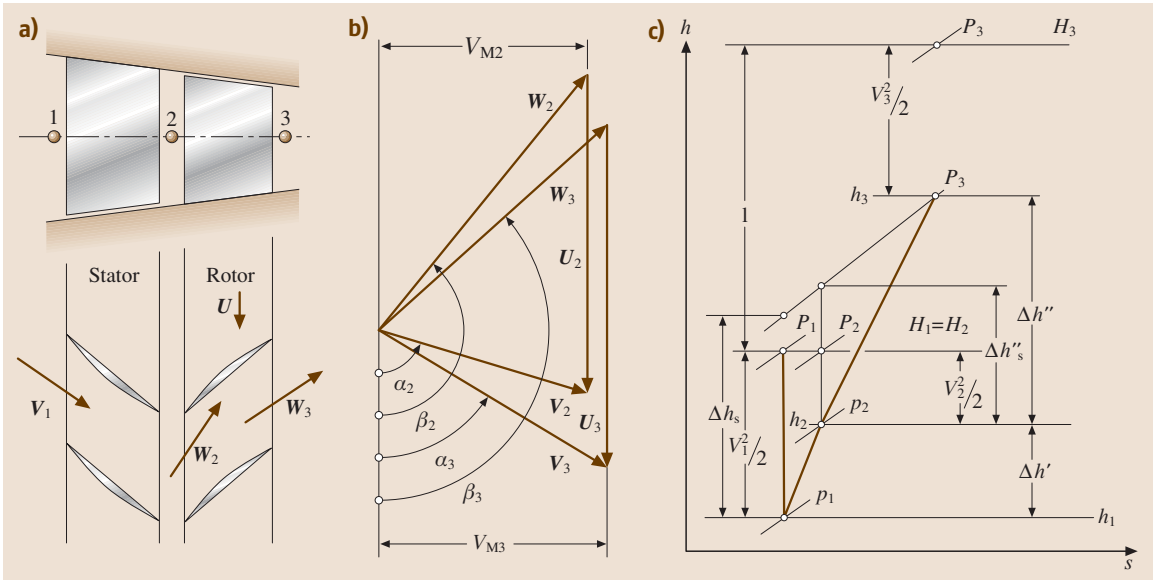


**Fig. 12.6a–c** A compressor stage (a) with the velocity diagram (b) and the expansion process (c). The direction of the unit vector $\boldsymbol{e}_1$ is identical with the rotational direction

literature $l_m = U_2 V_{u2} - U_3 V_{u3}$. In order to avoid confusion that may arise from different signs, it should be pointed out that the negative sign is the result of the formal derivation of the conservation law of moment of momentum. This negative sign implies that $V_{u1}$ and $V_{u2}$ point in the same direction. The unified angle convention introduced in Figs. 12.1 and 12.2, however, takes the actual direction of the velocity components with regard to a predefined coordinate system.

### 12.1.4 Dimensionless Stage Parameters

Equation (12.11) exhibits the direct relation between the specific stage work $l_m$ and the kinetic energies. The velocities from which these kinetics energies are built can be taken from the corresponding stage velocity diagram. The objective of this chapter is to introduce dimensionless stage parameters that completely determine the stage velocity diagram. These stage parameters exhibit unified relations for compressor and turbine stages, respectively.

Starting from a turbine or compressor stage with constant mean diameter and axial components (Fig. 12.7) we define the dimensionless stage parameters that describe the stage velocity diagram of a *normal stage* introduced by *Traupel* [12.3]. A normal stage is encountered within the high-pressure (HP) part of multistage turbines or compressor components and is characterized by $U_3 = U_2$, $V_3 = V_1$, $V_{m1} = V_{m3}$, and $\alpha_1 = \alpha_3$. The similarity of the velocity diagrams allows the same blade profile to be used throughout the HP turbine or compressor, thus significantly reducing manufacturing costs. We define the stage flow coefficient $\phi$ as the ratio of the meridional velocity component and the circumferential component. For this particular case, the meridional component is identical with the axial component

$$\phi = \frac{V_{m3}}{U_3} \,. \tag{12.12}$$

The stage flow coefficient $\phi$ in (12.12) is a characteristic of the mass flow behavior through the stage. The *stage load coefficient* $\lambda$ is defined as the ratio of the specific stage mechanical energy $l_m$ and the exit circumferential kinetic energy $U_3^2$. This coefficient directly relates the flow deflection given by the velocity diagram with the specific stage mechanical energy

$$\lambda = \frac{l_m}{U_3^2} \,. \tag{12.13}$$

The stage load coefficient $\lambda$ in (12.13) describes the work capability of the stage. It is also a measure for the stage loading. The *stage enthalpy coefficient* $\Psi$ represents the ratio of the isentropic stage mechanical energy and the exit circumferential kinetic energy $U_3^2$

$$\Psi = \frac{l_s}{U_3^2} \,. \tag{12.14}$$

The stage enthalpy coefficient represents the stage isentropic enthalpy difference within the stage. Furthermore, we define the *stage degree of reaction* $r$ which is the ratio of the static enthalpy difference used in the rotor row divided by the static enthalpy difference used in the entire stage

$$r = \frac{\Delta h''}{\Delta h'' + \Delta h'} \,. \tag{12.15}$$

The degree of reaction $r$ indicates the portion of energy transferred in the rotor blading. Using (12.5) and (12.6), we arrive at

$$r = \frac{\Delta h''}{\Delta h' + \Delta h''} = \frac{W_3^2 - W_2^2 + U_2^2 - U_3^2}{W_3^2 - W_2^2 + U_2^2 - U_3^2 + V_2^2 - V_1^2} \,. \tag{12.16}$$

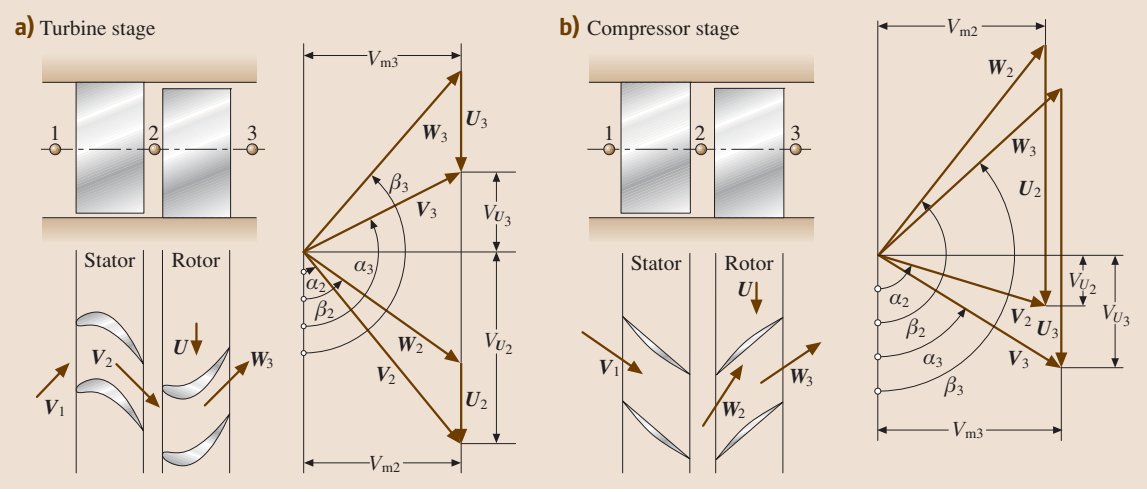


**Fig. 12.7a,b** Turbine (a) and compressor (b) stages with corresponding velocity diagrams

Since for the stage type under consideration, $V_1 = V_3$ and $U_2 = U_3$, (12.16) can be simplified as

$$r = \frac{W_3^2 - W_2^2}{W_3^2 - W_2^2 + V_2^2 - V_3^2} \,. \tag{12.17}$$

The velocity vectors and the corresponding kinetic energies are determined from the stage velocity diagram in connection with the angle and direction convention as follows

$$\begin{aligned} V_2 &= e_1(W_{u2} + U_2) + e_2 W_{m2} \,, \\ V_2^2 &= (W_{u2} + U_2)^2 + W_{m2}^2 \,, \\ V_3 &= e_1(W_{u3} + U_3) + e_2 W_{m3} \,, \\ V_3^2 &= (W_{u3} + U_3)^2 + W_{m3}^2 \,, \end{aligned} \tag{12.18}$$

since $U_2 = U_3 = U$ ,

$$V_2^2 - V_3^2 = W_2^2 - W_3^2 + 2UW_{u2} + 2UW_{u3} \,. \tag{12.19}$$

Using (12.18) and (12.19), (12.17) gives

$$r = \frac{W_3^2 - W_2^2}{2U(W_{u2} + W_{u3})} = \frac{W_{u3}^2 - W_{u2}^2}{2U(W_{u2} + W_{u3})} \,. \tag{12.20}$$

Rearranging (12.20) yields the final relationship for the particular stage we introduced above

$$r = \frac{1}{2}\frac{W_{u3} - W_{u2}}{U} \,. \tag{12.21}$$

### 12.1.5 Relation Between Degree of Reaction and Blade Height for a Normal Stage Using Simple Radial Equilibrium

In axial flow compressors or turbines, the working fluid has a rotational and translational motion. The rotating fluid is subjected to centrifugal forces that must be balanced by the pressure gradient in order to maintain the radial equilibrium. Consider an infinitesimal sector of an annulus with unit depth containing the fluid element which is rotating with tangential velocity $V_u$.

The centrifugal force acting on the element is shown in Fig. 12.8. Since the fluid element is in radial equilibrium, the centrifugal force is obtained from

$$\mathrm{d}F = \mathrm{d}m\frac{V_u^2}{R} \tag{12.22}$$

with $\mathrm{d}m = \rho R\,\mathrm{d}R\,\mathrm{d}\phi$. The centrifugal force is kept in balance by the pressure forces

$$\frac{\mathrm{d}\rho}{\mathrm{d}R} = p\frac{\mathrm{d}p}{\mathrm{d}\rho}\frac{V_u^2}{R} \,. \tag{12.23}$$

This result can also be obtained by decomposing the Euler equation of motion [12.1, Chap. 3, Eq. (3.46)] for inviscid flows into its three components in a cylindrical coordinate system. The Euler equation is expressed as

$$\boldsymbol{V} \cdot \nabla \boldsymbol{V} = -\frac{1}{\rho}\nabla p \,. \tag{12.24}$$

In the radial direction

$$V_r\frac{\partial V_r}{\partial R} + V_u\frac{\partial V_r}{R\partial\varphi} + V_z\frac{\partial V_r}{\partial z} - \frac{V_u^2}{R} = -\frac{1}{\rho}\frac{\partial p}{\partial R} \,. \tag{12.25}$$

The assumptions needed to arrive at (12.23) are

$$\frac{\partial V_r}{\partial R} \simeq 0 \,, \text{ axial symmetric: } \frac{\partial V_r}{\partial \varphi} = 0 \,, \quad \frac{\partial V_r}{\partial z} \simeq 0 \,. \tag{12.26}$$

With these assumptions, (12.24) yields

$$\frac{1}{\rho}\frac{\partial p}{\partial R} = \frac{V_u^2}{R} \,. \tag{12.27}$$

Equation (12.27) is identical with (12.23). Calculation of a static pressure gradient requires additional information from the total pressure relation. For this purpose, we apply the Bernoulli equation neglecting the gravitational term

$$P = p + \frac{1}{2}\rho V^2 = p + \frac{1}{2}\rho\left(V_u^2 + V_{ax}^2\right) \,. \tag{12.28}$$

Using (12.28), the change in radial direction is

$$\frac{\mathrm{d}p_0}{\mathrm{d}R} = \frac{\mathrm{d}p}{\mathrm{d}R} + \rho V_u\frac{\mathrm{d}V_u}{\mathrm{d}R} + \rho V_{ax}\frac{\mathrm{d}V_{ax}}{\mathrm{d}R} \,. \tag{12.29}$$

If the stagnation or total pressure $P = p_0 = \text{const}$ and $V_{ax} = \text{const}$, (12.29) yields

$$\frac{\mathrm{d}p}{\mathrm{d}R} + \rho V_u\frac{\mathrm{d}V_u}{\mathrm{d}R} = 0 \,, \quad \text{or} \quad \frac{\mathrm{d}p}{\mathrm{d}R} = -\rho V_u\frac{\mathrm{d}V_u}{\mathrm{d}R} \,. \tag{12.30}$$

Equating (12.30) and (12.23) results in

$$V_u\frac{\mathrm{d}V_u}{\mathrm{d}R} + \frac{V_u^2}{R} = 0 \tag{12.31}$$

or

$$\frac{\mathrm{d}V_u}{V_u} + \frac{\mathrm{d}R}{R} = 0 \,. \tag{12.32}$$

The integration of (12.32) leads to $V_u R = \text{const}$. This type of flow is called free vortex flow and fulfills the requirement to be potential flow, $\nabla \times V = 0$. We use

this relation to rearrange the specific stage mechanical energy

$$l_m = U_2 V_{u2} + U_3 V_{u3} = \omega(R_2 V_{u2} + R_3 V_{u3}) \,. \quad (12.33)$$

At station 2 the swirl is $R_2 V_{u2} = \text{const} = K_2$; likewise at station 3 the swirl is $R_3 V_{u3} = K_3$. Since $\omega = \text{const}$, the specific stage mechanical energy is constant

$$l_m = (K_2 + K_3)\omega = \text{const} \,. \quad (12.34)$$

Equation (12.34) implies that, for a stage with constant spanwise meridional components and constant total pressure from hub to tip, the specific stage mechanical energy is constant over the entire blade height. To express the degree of reaction in the spanwise direction, we replace the enthalpy differences in (12.15) by pressure differences. For this purpose we apply the first law for an adiabatic process through stator and rotor blades expressed in terms of $\Delta h'' = \bar{v}'' \Delta p''$ and $\Delta h' = \bar{v}' \Delta p'$. This leads to

$$r = \frac{\bar{v}'' \Delta p''}{\bar{v}'' \Delta p'' + \bar{v}' \Delta p'} = \frac{\Delta p''}{\Delta p'' + \frac{\bar{v}'}{\bar{v}''} \Delta p'} \simeq \frac{p_2 - p_3}{p_1 - p_3} \,. \quad (12.35)$$

In (12.35), the ratio of specific volumes was approximated as $\bar{v}'/\bar{v}'' \simeq 1$. This approximation is admissible for low Mach number ranges. Considering $R_2 V_{u2} = \text{const}$, the integration of (12.23) for station 1 from an arbitrary diameter $R$ to the mean diameter $R_m$ yields

$$(p_1 - p_{m1}) = \frac{\rho}{2}(V_{um})_1^2 \left(1 - \frac{R_m^2}{R^2}\right)_1 \,. \quad (12.36)$$

At station 2 we have

$$(p_2 - p_{m2}) = \frac{\rho}{2}(V_{um})_2^2 \left(1 - \frac{R_m^2}{R^2}\right)_2 \quad (12.37)$$

and finally, at station 3 we arrive at

$$(p_3 - p_{m3}) = \frac{\rho}{2}(V_{um})_3^2 \left(1 - \frac{R_m^2}{R^2}\right)_3 \,, \quad (12.38)$$

with $(R_m)_1 = (R_m)_2 = (R_m)_3$ and $V_{um3} = V_{um1}$. Introducing (12.36)–(12.38) into (12.35), we finally arrive at a simple relationship for the degree of reaction

$$\frac{1-r}{1-r_m} - \frac{R_m^2}{R^2} \,. \quad (12.39)$$

From a turbine design point of view, it is of interest to estimate the degree of reaction at the hub and tip radius by inserting the corresponding radii into (12.39). As a result, we find

$$\frac{1-r_h}{1-r_m} = \left(\frac{R_m}{R_h}\right)^2 \,, \quad \frac{1-r_t}{1-r_m} = \left(\frac{R_m}{R_t}\right)^2 \,. \quad (12.40)$$

Equation (12.40) represents a simple radial equilibrium condition which allows the calculation of the inlet flow angle in a radial direction by integrating (12.32)

$$V_u R = \text{const} \,, \quad R = \frac{\text{const}}{V_u} \,. \quad (12.41)$$

This leads to the determination of the inlet flow angle in a spanwise direction as

$$\frac{R_m}{R} = \frac{\cot\alpha_1}{\cot\alpha_m} \,. \quad (12.42)$$

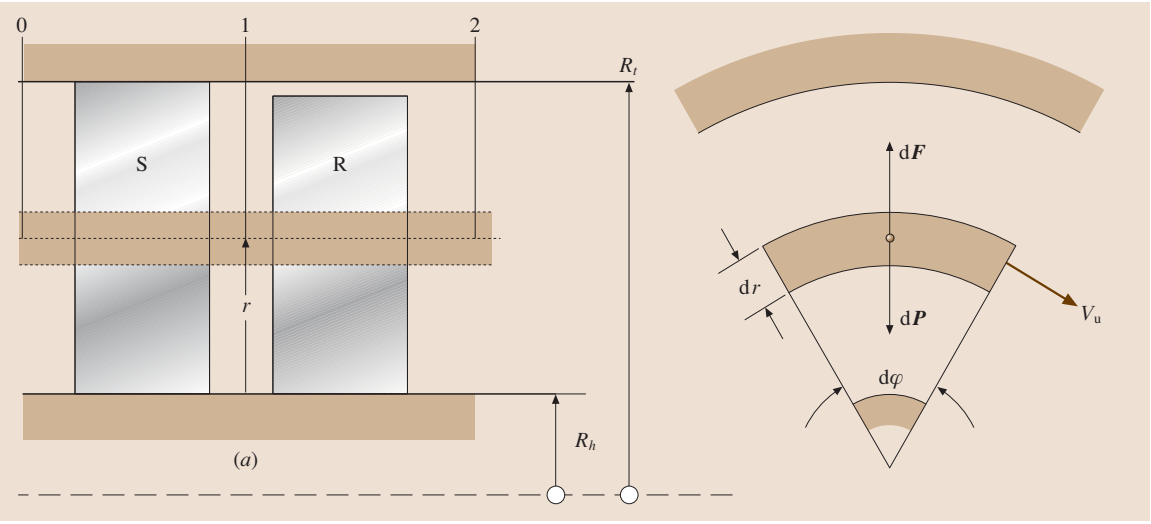


**Fig. 12.8** Explanation for simple radial equilibrium

### 12.1.6 Effect of Degree of Reaction on the Stage Configuration

The distribution of degree of reaction can also be obtained simply by using the velocity ratio for $r$. If, for example, the degree of reaction at the mean diameter is set at $r = 50\%$, (12.40) immediately calculates $r$ at the hub and tip for the simple radial equilibrium condition $V_u R = \text{const}$, as presented above. It should be mentioned that for a turbine a negative degree of reaction at the hub may lead to flow separation and is not desired. Likewise, for a compressor, $r$ should not exceed the value of 100%. The value of $r$ has major design consequences. For turbine blades with $r = 0$, as shown in Figs. 12.9a and 12.10, the flow is deflected in the rotor and exit velocity vectors have the same magnitude but opposite directions. The entire stage static enthalpy difference is partially converted within the stator row. Note that the flow channel cross section remains constant. For $r = 0.5$, shown in Fig. 12.9b, a fully symmetric blade configuration is established. Figure 12.9c shows a turbine stage with $r > 0.5$. In this case, the flow deflection inside the rotor row is much greater than the one inside the stator row. Figure 12.10 shows the flow deflection within a high-speed rotor cascade. In the past, mainly two types of stages were common designs in steam turbines. The stage with a constant pressure across the rotor blading ($p_2 = p_3$), called an *action stage*, was used frequently. This turbine stage was designed such that the exit absolute velocity vector $V_3$ was swirl free. It is most appropriate for the design of single-stage turbines and as the last stage of a multistage turbine. The *exit loss*, which corresponds to the kinetic energy of the exiting mass flow, becomes a minimum by using a swirl-free absolute velocity. The stage with $r = 0.5$ is called the *reaction stage*.

### 12.1.7 Effect of the Stage Load Coefficient on Stage Power

The stage load coefficient $\lambda$ defined in (12.13) is an important parameter, which describes the capability of the stage to generate/consume shaft power. A turbine stage with low flow deflection, and thus low specific stage load coefficient $\lambda$, generates lower specific mechanical energy. To increase the stage mechanical energy $l_m$, blades with higher flow deflection are used that produce higher stage load coefficient $\lambda$. The effect of an increased $\lambda$ is shown in Fig. 12.11, where three different bladings are plotted.

The top blading with the stage load coefficient $\lambda = 1$ has lower deflection. The middle blading has a moderate flow deflection and moderate $\lambda = 2$, which delivers twice as much stage power as the top blading. Finally, the bottom blading with $\lambda = 3$ delivers three times the stage power as the first one. In the practice of turbine design, among other things, two major parameters must be considered: the specific load coefficients and the stage polytropic efficiencies.

Lower deflection generally yields higher stage polytropic efficiency, but many stages are needed to produce the required turbine power. However, the same turbine

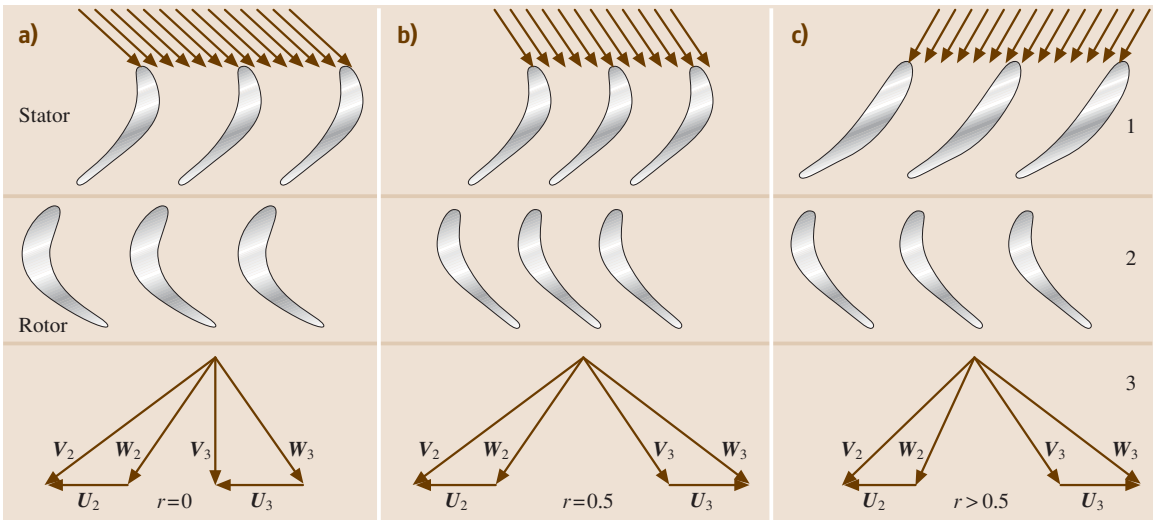


**Fig. 12.9a–c** Effect of degree of reaction on the stage configuration

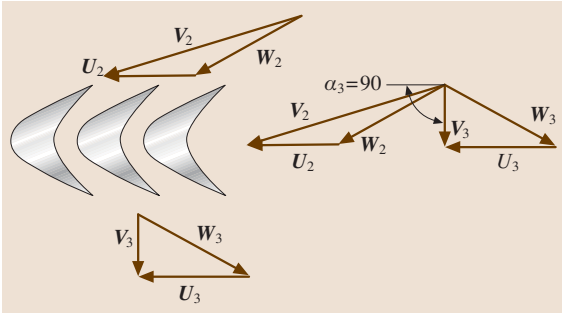


**Fig. 12.10** Flow through a high-speed turbine rotor with a degree of reaction $r = 0.0$, note that $\alpha_3 = 90°$ and $|\boldsymbol{W}_2| = |\boldsymbol{W}_3|$

power may be established by a higher stage flow deflection, and thus a higher λ, at the expense of the stage efficiency. Increasing the stage load coefficient has the advantage of significantly reducing the stage number, thus lowering the engine weight and manufacturing cost. In aircraft engine design practice, one of the most critical issues besides the thermal efficiency of the engine is the thrust-to-weight ratio. Reducing the number of stages may lead to a desired thrust-to-weight ratio. While a high turbine stage efficiency has top priority in power generation steam and gas turbine design, the thrust-to-weight ratio is the major parameter for aircraft engine designers.

### 12.1.8 Unified Description of a Turbomachinery Stage

The following sections treat turbine and compressor stages from a unified standpoint. Axial, mixed flow, and radial flow turbines and compressors follow the same thermodynamic conservation principles. Special treatments are indicated when dealing with aerodynamic behavior and loss mechanisms. While turbine aerodynamics is characterized by negative (favorable) pressure gradient environments, the compression process operates in a positive (adverse) pressure gradient environment. As a consequence, partial or total flow separation may occur on compressor blade surfaces, leading to partial stall or surge. On the other hand, with the exception of some minor local separation bubbles on the suction surface of highly loaded low-pressure turbines blades, a turbine normally operates without major flow separation or breakdown. These two distinctively different aerodynamic behaviors are due to the different pressure gradient environments. Turbine and compressor cascade aerodynamics and losses are extensively treated in [12.1, Chaps. 7 and 16]. In this section, we will first present a set of algebraic equations that describes turbine and compressor stages with constant mean diameter and then extend the approach to general cases where the mean stage diameter changes.

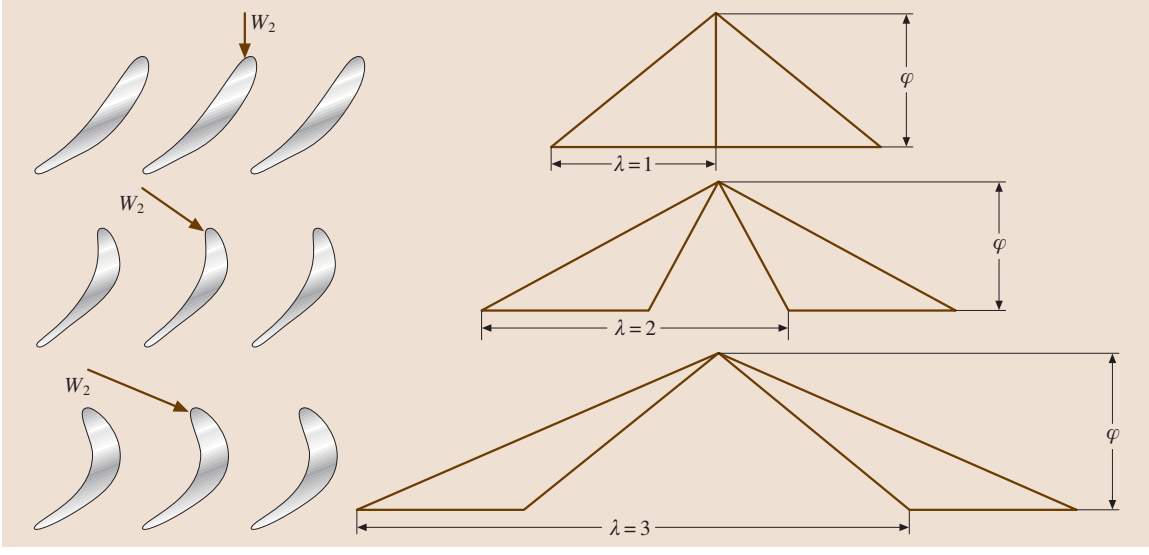


**Fig. 12.11** Dimensionless stage velocity diagram to explain the effect of the stage load coefficient λ on flow deflection and blade geometry, $r = 0.5$

### Unified Description of Stages with Constant Mean Diameter

For a turbine or compressor stage with constant mean diameter (Fig. 12.7), we present a set of equations that describe the stage by means of dimensionless parameters such as stage flow coefficient $\phi$, stage load coefficient $\lambda$, degree of reaction $r$, and the flow angles. From the velocity diagram with the angle definition in Fig. 12.7, we obtain the flow angles

$$\begin{aligned}\cot\alpha_2 &= \frac{U_2 + W_{u2}}{V_{ax}} = \frac{1}{\phi}\left(1 + \frac{W_{u2}}{U}\right)\\ &= \frac{1}{\phi}\left(1 - r + \frac{\lambda}{2}\right),\\ \cot\alpha_3 &= -\frac{W_{u2} - U_2}{V_{ax}} = -\frac{1}{\phi}\left(\frac{W_{u3} - U}{U}\right)\\ &= \frac{1}{\phi}\left(1 - r - \frac{\lambda}{2}\right). \end{aligned} \tag{12.43}$$

The other flow angles can be found similarly, thus we summarize

$$\cot\alpha_2 = \frac{1}{\phi}\left(1 - r + \frac{\lambda}{2}\right), \tag{12.44}$$

$$\cot\alpha_3 = \frac{1}{\phi}\left(1 - \frac{\lambda}{2} - r\right), \tag{12.45}$$

$$\cot\beta_2 = \frac{1}{\phi}\left(\frac{\lambda}{2} - r\right), \tag{12.46}$$

$$\cot\beta_3 = -\frac{1}{\phi}\left(\frac{\lambda}{2} + r\right). \tag{12.47}$$

The stage load coefficient can be calculated from

$$\lambda = \phi(\cot\alpha_2 - \cot\beta_3) - 1\,. \tag{12.48}$$

The velocity diagram of the last stage of a compressor or a turbine differs considerably from the normal stage. As mentioned in the previous section, to minimize the *exit losses*, the last stage usually has an exit flow angle of $\alpha_3 = 90°$. Figure 12.12 compares the velocity diagram of a normal stage with the one in the last stage of the same turbine component. As shown, by changing the exit flow angle to $\alpha_3 = 90°$ a substantial reduction in exit velocity vector $V_3$, and thus the exit kinetic energy $V_3^2$, can be achieved. This subject is treated in [12.1, Chap. 7] in detail.

### Generalized Dimensionless Stage Parameters

Now we extend the foregoing consideration to compressor and turbine stages where the diameter, circumferential velocities, and meridional velocities are not constant. Examples are axial flow turbine and compressors (Figs. 12.5 and 12.6), radial inflow (centripetal) turbines (Fig. 12.13), and centrifugal compressors (Fig. 12.14).

In the following, we develop a set of unifying equations that describes the above axial turbine and compressor stages, as well as the centripetal turbine and centrifugal compressor stages shown in Figs. 12.13 and 12.14. We introduce new dimensionless parameters

$$\mu = \frac{V_{m2}}{V_{m3}}\,,\quad \nu = \frac{R_2}{R_3} = \frac{U_2}{U_3}\,,\quad \phi = \frac{V_{m3}}{U_3}\,,\quad \lambda = \frac{l_m}{U_3^2}\,,$$
$$r = \frac{\Delta h''}{\Delta h' + \Delta h''}\,, \tag{12.49}$$

with $V_m$, $U$ from the velocity diagrams and $\Delta h'$ and $\Delta h''$ as the specific static enthalpy difference in the rotor and stator, respectively. The dimensionless parameters $\mu$ represents the meridional velocity ratio for the stator and rotor, respectively, $\nu$ is the circumferential velocity ratio, $\phi$ is the stage flow coefficient, $\lambda$ is the stage load coefficient, and $r$ is the degree of reaction. Introducing these parameters into the equations of continuity, moment of momentum, and the relation for degree of reaction, the stage is completely defined by a set of four

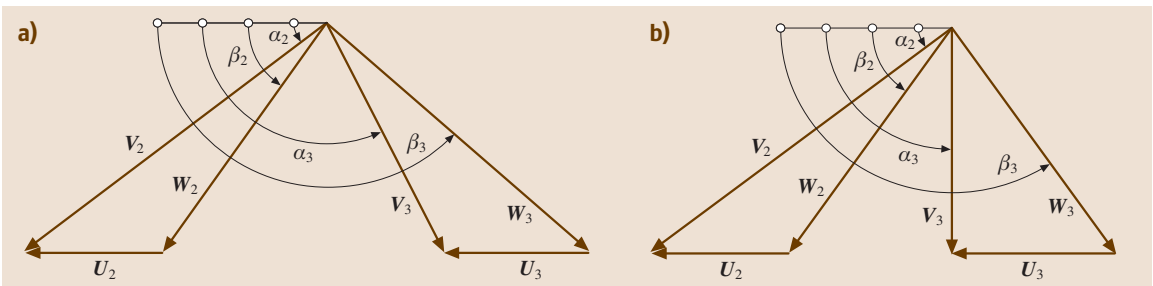


**Fig. 12.12a,b** Turbine stage velocity diagrams: **(a)** for a normal stage, and **(b)** for the last stage of a multistage turbine

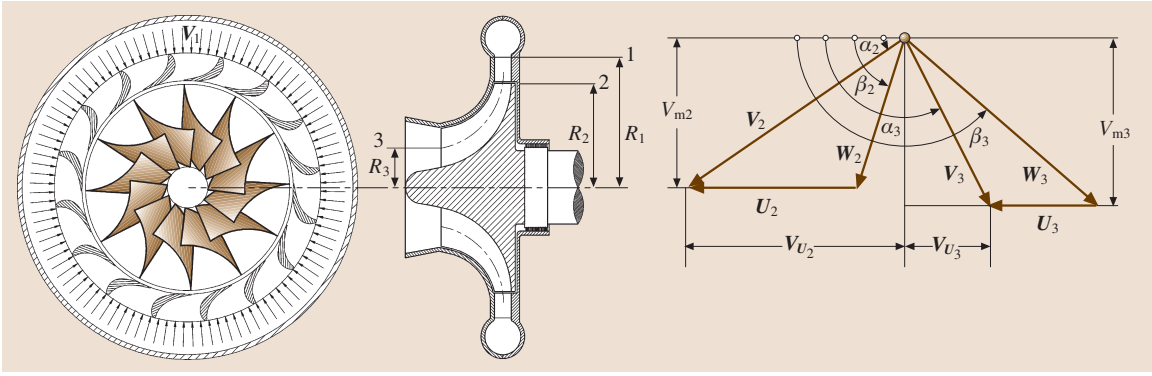


**Fig. 12.13** A centripetal turbine stage with cross section and velocity diagram

equations

$$\cot\alpha_2 - \cot\beta_2 = \frac{\nu}{\mu\,\phi}\,, \tag{12.50}$$

$$\cot\alpha_3 - \cot\beta_3 = \frac{1}{\phi}\,, \tag{12.51}$$

$$r = 1 + \frac{\phi^2}{2\lambda}\left[1 + \cot^2\alpha_3 - \mu^2\left(1 + \cot^2\alpha_2\right)\right], \tag{12.52}$$

$$\lambda = \phi(\mu\nu\cot\alpha_2 - \cot\beta_3) - 1\,. \tag{12.53}$$

While (12.50), (12.51) and (12.53) are exact, (12.52) is only an approximation. However, its exact value can be obtained by solving equation system (12.54). The system of (12.50–12.53) contains nine unknown stage parameters. To find a solution, five parameters must be guessed. Appropriate candidates for the first guess are: the diameter ratio, $\nu = R_2/R_3 = U_2/U_3$, the stator and rotor exit angles $\alpha_2$ and $\beta_3$, the exit flow angle $\alpha_3$, and the stage degree of reaction $r$. In addition, the stage flow coefficient $\phi$ can be estimated by implementing the information about the mass flow and using the continuity equation. Likewise, the stage load coefficient $\lambda$ can be estimated for turbine or compressor stages by employing the information about the compressor pressure ratio or turbine power. Once the five parameters are guessed, the rest of the four parameters are determined by solving the above equation system. In this case, the four parameters calculated fulfill the conservation laws for the particular compressor or turbine blade geometry for which the five stage parameters were guessed. This preliminary estimation of stage parameters, however, is considered the first iteration toward an optimum design. A subsequent loss and efficiency calculation, presented in [12.1, Chap. 8], will clearly show if the guessed parameters were useful or not. In fact, a few iterations are necessary to find the optimum configuration that fulfills the efficiency requirement set by

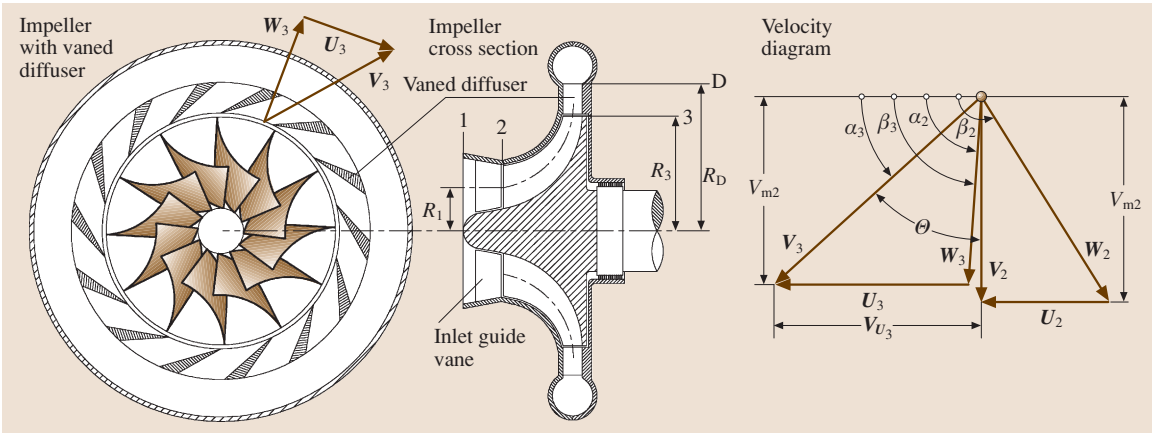


**Fig. 12.14** A centrifugal compressor stage with cross section and velocity diagram

the compressor or turbine designer. Equations (12.50–12.53) can be expressed in terms of the flow angles $\alpha_2$, $\alpha_3$, $\beta_2$, and $\beta_3$, which lead to a set of four nonlinear equations

$$\begin{aligned}
&\mu^2\phi^2(1-\nu^2)\cot^2\alpha_2 + 2\mu\nu\,\phi\,\lambda\cot\alpha_2 - \lambda^2 \\
&\quad - 2(1-r)\lambda + (\mu^2-1)\phi^2 = 0\,, \\
&\phi^2(1-\nu^2)\cot^2\alpha_3 + 2\phi\,\lambda\cot\alpha_3 + \lambda^2 \\
&\quad - 2(1-r)\lambda\nu^2 + (\mu^2-1)\phi^2\nu^2 = 0\,, \\
&(1-\nu^2)(\mu\,\phi\cot\beta_2 + \nu)^2 + 2\nu\,\lambda(\phi\,\mu\cot\beta_2 + \nu) - \lambda^2 \\
&\quad - 2(1-r)\lambda + (\mu^2-1)\phi^2 = 0\,, \\
&(1-\nu^2)(\phi\cot\beta_3 + 1)^2 + 2\lambda(\phi\cot\beta_3 + 1) + \lambda^2 \\
&\quad - 2(1-r)\lambda\nu^2 + (\mu^2-1)\phi^2\nu^2 = 0\,.
\end{aligned} \tag{12.54}$$

### 12.1.9 Special Cases

Equations (12.50–12.54) are equally valid for axial, radial, and mixed flow turbine and compressor stages. Special stages with corresponding dimensionless parameters are described as special cases as listed below.

#### Case 1: Constant Mean Diameter

In this special case, the diameter remains constant, leading to the circumferential velocity ratio of $\nu = U_2/U_3 = 1$. The meridional velocity ratio is $\mu = V_{m2}/V_{m3} \neq 1$. The flow angles expressed in terms of other dimensionless parameters are

$$\begin{aligned}
\cot\alpha_2 &= \frac{1}{\phi\,\mu}\left[\frac{\lambda}{2} + (1-r) - (\mu^2-1)\frac{\phi^2}{2\lambda}\right], \\
\cot\alpha_3 &= \frac{1}{\phi}\left[-\frac{\lambda}{2} - (1-r) - (\mu^2-1)\frac{\phi}{2\lambda}\right], \\
\cot\beta_2 &= \frac{1}{\mu\,\phi}\left[\frac{\lambda}{2} + (1-r) - (\mu^2-1)\frac{\phi^2}{2\lambda} - 1\right], \\
\cot\beta_3 &= \frac{1}{\phi}\left[-\frac{\lambda}{2} + (1-r) - (\mu^2-1)\frac{\phi}{2\lambda} - 1\right].
\end{aligned} \tag{12.55}$$

The stage load coefficient is calculated from

$$\lambda = \phi(\mu\cot\alpha_2 - \cot\beta_3) - 1 \quad \text{for } \nu = 1 \text{ and } \mu \neq 1\,. \tag{12.56}$$

#### Case 2: Constant Mean Diameter and Meridional Velocity Ratio

In this special case, the circumferential and meridional velocities are equal, leading to $\nu = U_2/U_3 = 1$, $\mu = V_{m2}/V_{m3} = 1$. The flow angles are calculated from

$$\begin{aligned}
\cot\alpha_2 &= \frac{1}{\phi}\left(\frac{\lambda}{2} - r + 1\right), \\
\cot\alpha_3 &= \frac{1}{\phi}\left(-\frac{\lambda}{2} - r + 1\right).
\end{aligned} \tag{12.57}$$

The stage load coefficient is calculated from

$$\lambda = \phi(\cot\alpha_2 - \cot\beta_3) - 1 \quad \text{for } \nu = 1 \text{ and } \mu = 1\,. \tag{12.58}$$

The generalized stage load coefficient for different $\mu$, $\nu$-cases can be summarized as

$$\begin{aligned}
\lambda &= \phi[\mu\nu\cot\alpha_2 - \cot\beta_3] - 1 \quad \text{for } \nu \neq 1 \text{ and } \mu \neq 1\,, \\
\lambda &= \phi[\mu\cot\alpha_2 - \cot\beta_3] - 1 \quad \text{for } \nu = 1 \text{ and } \mu \neq 1\,, \\
\lambda &= \phi[\nu\cot\alpha_2 - \cot\beta_3] - 1 \quad \text{for } \nu \neq 1 \text{ and } \mu = 1\,, \\
\lambda &= \phi[\cot\alpha_2 - \cot\beta_3] - 1 \quad \text{for } \nu = 1 \text{ and } \mu = 1\,.
\end{aligned} \tag{12.59}$$

### 12.1.10 Increase of Stage Load Coefficient: Discussion

Following the discussion in Sect. 12.1.3 regarding the increase of the specific stage mechanical energy and the subsequent discussion in Sect. 12.1.8, we proceed with (12.53), where the stage load parameter $\lambda$ is expressed in terms of $\mu$ and $\nu$ and the blade angle $\alpha_2$ and $\beta_3$ as

$$\lambda = \phi(\mu\nu\cot\alpha_2 - \cot\beta_3) - 1\,. \tag{12.60}$$

The effect of flow deflection on the stage load coefficient of axial flow turbines was already discussed in Sect. 12.1.8. As we saw, turbine blades can be designed with stage load coefficients $\lambda$ as high as 3 or more. In turbine blades with high $\lambda$ and Reynolds numbers $\mathrm{Re} = V_{exit}\,c/\nu > 150\,000$, the governing strong negative pressure gradient prevents major separation from occurring in the flow. However, if the same type of blade operates at lower Reynolds numbers, flow separation that results in a noticeable increase of profile losses may occur. For high-pressure turbines (HPT), the strong favorable pressure gradient within the blade channels prevents major separation from occurring in the flow. However, low-pressure turbine (LPT) blades, particularly those of aircraft gas turbine engines that operate at low Reynolds numbers (cruise conditions up to $\mathrm{Re} = 120\,000$), are subjected to laminar flow separation and turbulent reattachment. While axial turbine blades can be designed with relatively high positive $\lambda$,

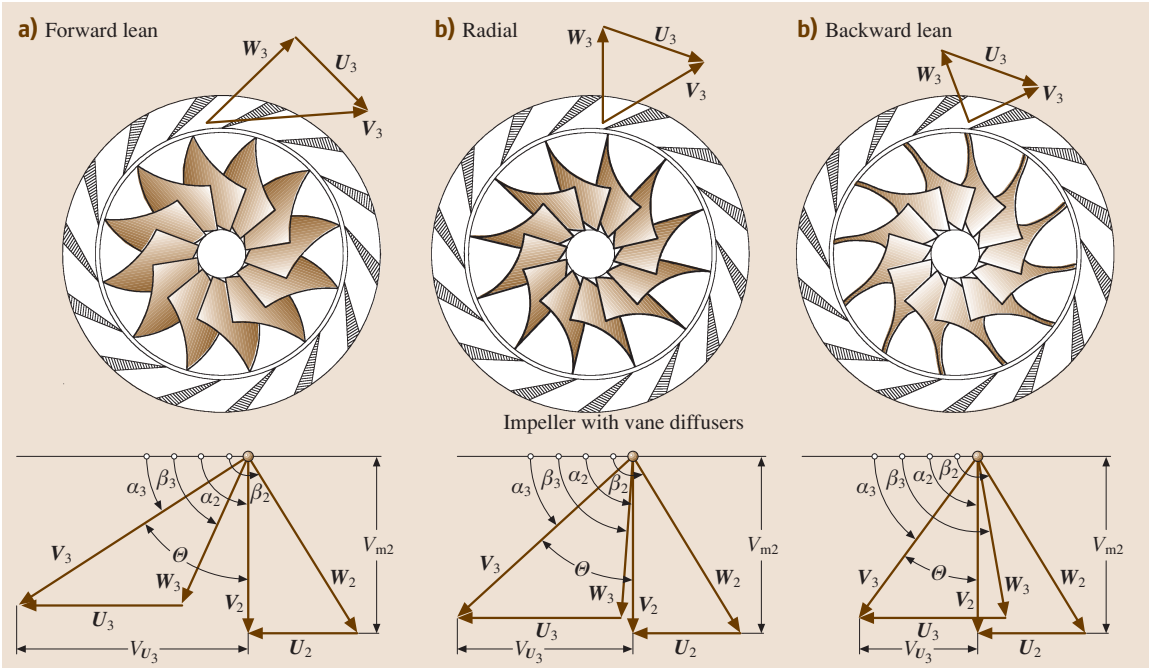


**Fig. 12.15a–c** Centrifugal compressor stage with velocity diagrams: **(a)** forward lean, **(b)** radial zero lean, and **(c)** backward lean

the flow through axial compressor blade channels is susceptible to flow separation, even at relatively low λ. This is primarily due to a positive pressure gradient in the streamwise direction that causes the boundary layer to separate once a certain deflection limit or a *diffusion factor* (see [12.1, Chap. 16]) has been exceeded. To achieve a higher λ, and thus a higher stage pressure ratio, a smaller diameter ratio $\nu = D_2/D_3 = U_2/U_3$ can be applied. Using a moderate diameter ratio range of $\nu = 0.85 - 0.75$ results in a mixed flow configuration. At a lower range of $\nu$, such as $\nu = 0.75 - 0.4$, a centrifugal compressor configuration is designed.

Figure 12.15 shows, schematically, three centrifugal compressors with three different exit flow angles and the corresponding velocity diagrams. Figure 12.15a shows a centrifugal impeller in which the trailing edge portion is forward leaning with a negative lean angle of $\Delta\beta = \beta_3 - 90° < 0$. The reference configuration Fig. 12.15b shows an impeller with a radial exit flow angle $\beta_3 = 90°$ and thus $\Delta\beta = 0$. Finally, Fig. 12.15c shows an impeller with a backward-leaned trailing edge portion with a positive lean angle of $\Delta\beta = \beta_3 - 90° > 0$. All three

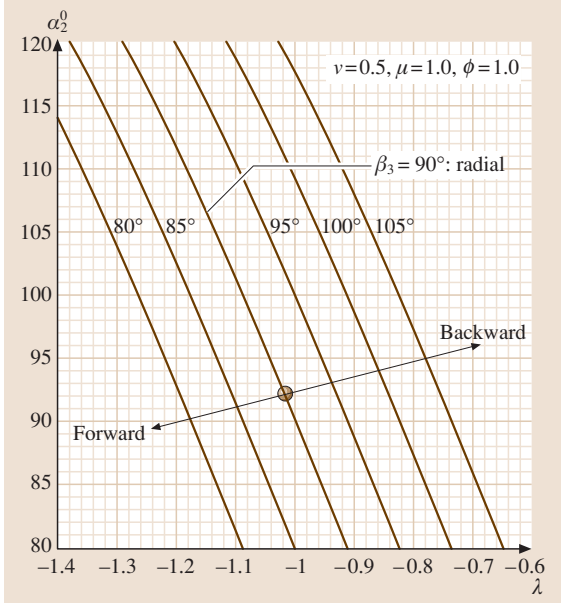


**Fig. 12.16** Influence of lean angle on λ: forward lean with $\beta_3 < 90°$, backward lean $\beta_3 > 90°$, and zero lean $\beta_3 = 90°$

impellers have the same diameter ratio $\nu$ and the same rotational speed $\omega$. The $\lambda$-behavior of these impellers is shown in Fig. 12.16, where the relative exit flow angle is varied in the range of $\beta_3 = 80° - 105°$. As shown, forward lean results in higher deflection $\Theta$, larger $\Delta V_u$, and thus higher negative $\lambda$, which is associated with a higher profile loss. Backward lean, however, reduces the flow deflection $\Theta$ and $\Delta V_u$. As a result, the stage load coefficient $\lambda$ is reduced. For the comparison, the radial exit case with $\beta_3 = 90°$ is plotted. In calculating the stage load coefficient $\lambda$, the influence of the radius ratio $\nu = R_2/R_3 = U_2/U_3$ on the stage load coefficient becomes clear.



## 12.2 Gas Turbine Engines: Design and Dynamic Performance

A gas turbine engine is a system that consists of several turbomachinery components and auxiliary subsystems. Air enters the compressor component, which is driven by a turbine component that is placed on the same shaft. Air exits the compressor at a higher pressure and enters the combustion chamber, where the chemical energy of the fuel is converted into thermal energy, producing combustion gas at a temperature that corresponds to the turbine inlet design temperature. The combustion gas expands in the following turbine component, where its total energy is partially converted into shaft work and exit kinetic energy. For power generation gas turbines, the shaft work is the major portion of the above energy forms. It covers the total work required by the compressor component, the bearing frictions, several auxiliary subsystems, and the generator. In aircraft gas turbines, a major portion of the total energy goes toward generation of high exit kinetic energy, which is essential for thrust generation.

Gas turbines are designed for particular applications that determine their design configurations. For power generation purposes, the gas turbine usually has a *single spool*. A spool combines a compressor and a turbine that are connected together via a shaft. Figure 12.17 exhibits a single-spool power generation gas turbine, where a 14-stage compressor shares the same shaft with a three-stage turbine.

While in power generation gas turbine design the power-to-weight ratio does not play an important role, the thrust-to-weight ratio is a primary parameter in designing an aircraft gas turbine. High-performance aircraft gas turbine engines generally have twin-spool or multispool arrangements. The spools are usually rotating at different angular velocities and are connected with each other aerodynamically via air or combustion gas. Figure 12.18 exhibits a typical high-performance twin-spool aircraft gas turbine with a *ducted front fan* as the main thrust generator. Gas turbine engines with power capacities less than 20 MW might have a *split shaft* configuration that consists of a *gas generation spool* and a *power shaft*. While the turbine of the gas generation spool provides the shaft work necessary to drive the compressor, the power shaft produces the net power. In addition to the above design configurations, a variety of engine derivatives can be constructed using a core engine as shown in Fig. 12.19.

### 12.2.1 Gas Turbine Processes, Steady Design Operation

Starting with the single-spool power generation gas turbine that consists of a multistage compressor, a combustion chamber, and a turbine, the $h$–$s$ diagram is shown in Fig. 12.20a.

The compression process from 1 to 2 is accomplished by the compressor with a polytropic efficiency $\eta_{pol}$ that can be accurately calculated using the row-by-row or stage-by-stage methods discussed in [12.6]. The combustion process from 2 to 3 is associated with certain total pressure loss coefficient $\zeta_{comb}$, thus it is not considered isobaric. The expansion process from 3 to 4 causes an entropy increase that is determined by the turbine efficiency. Figure 12.20b shows the $h$–$s$ diagram for a twin-spool aircraft engine. In contrast to the single-spool engine, the compression process is accomplished by two compressors that are operating at two different angular velocities. Air enters the low-pressure (LP) compressor driven by the LP turbine and is compressed from 1 to 2. Further compression from 2 to 3 occurs in the high-pressure compressor (HP compressor) driven by the HP turbine. After addition of fuel in the combustion chamber, the fist expansion occurs in the HP turbine, whose power exactly matches the sum of the HP compressor power and the power required to compensate bearing frictions. The second expansion in the LP turbine matches the power by the LP compressor, bearing friction, and the auxiliary subsystems. In off-design operation, there is always a dynamic

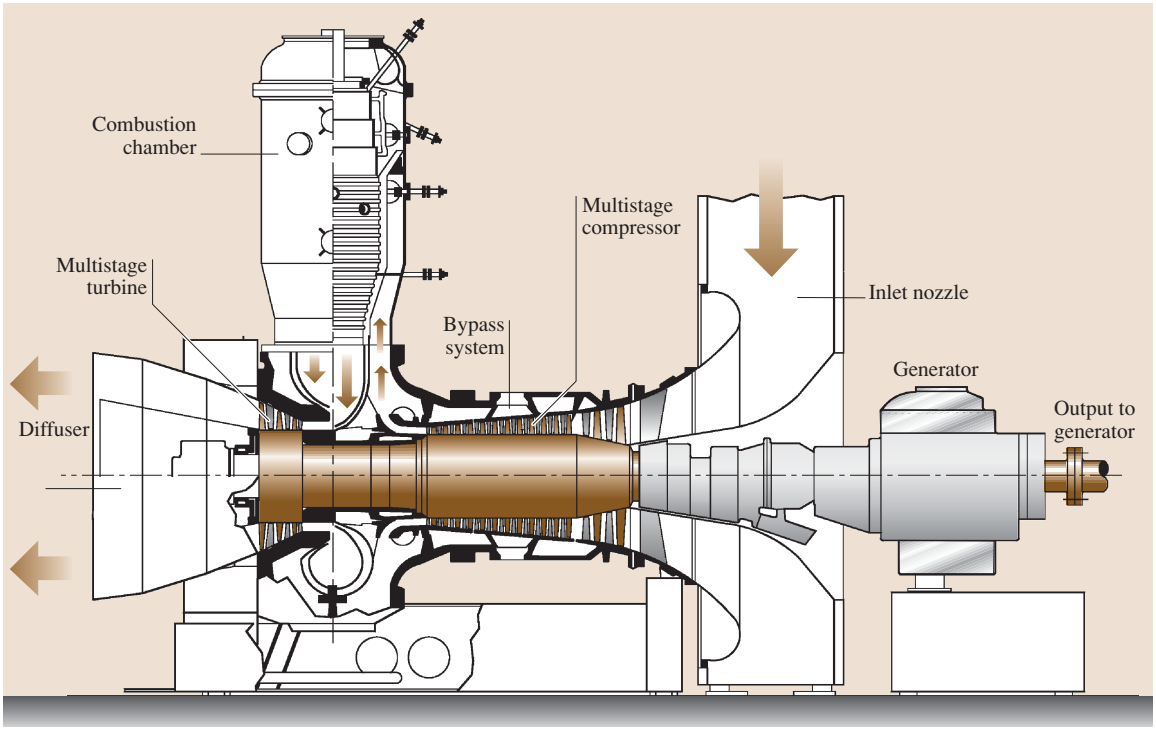


**Fig. 12.17** A single-spool power generation gas turbine BBC-GT9

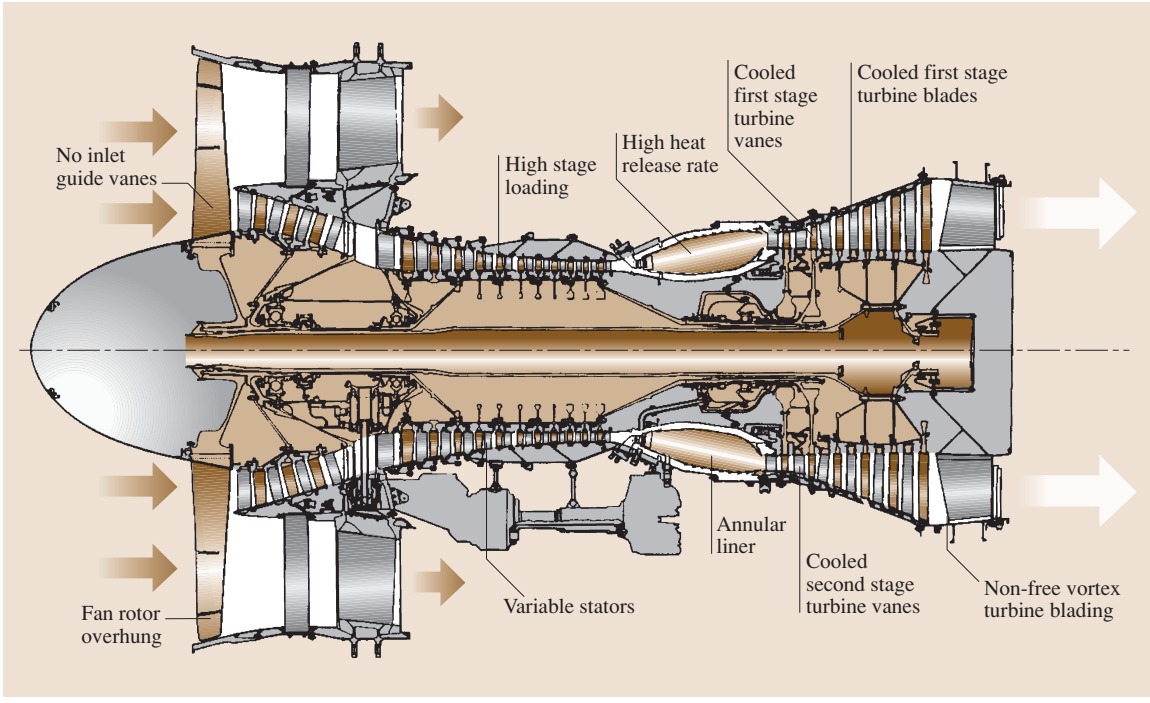


**Fig. 12.18** A twin-spool Pratt & Whitney high-bypass-ratio aircraft engine with multistage compressors and turbines

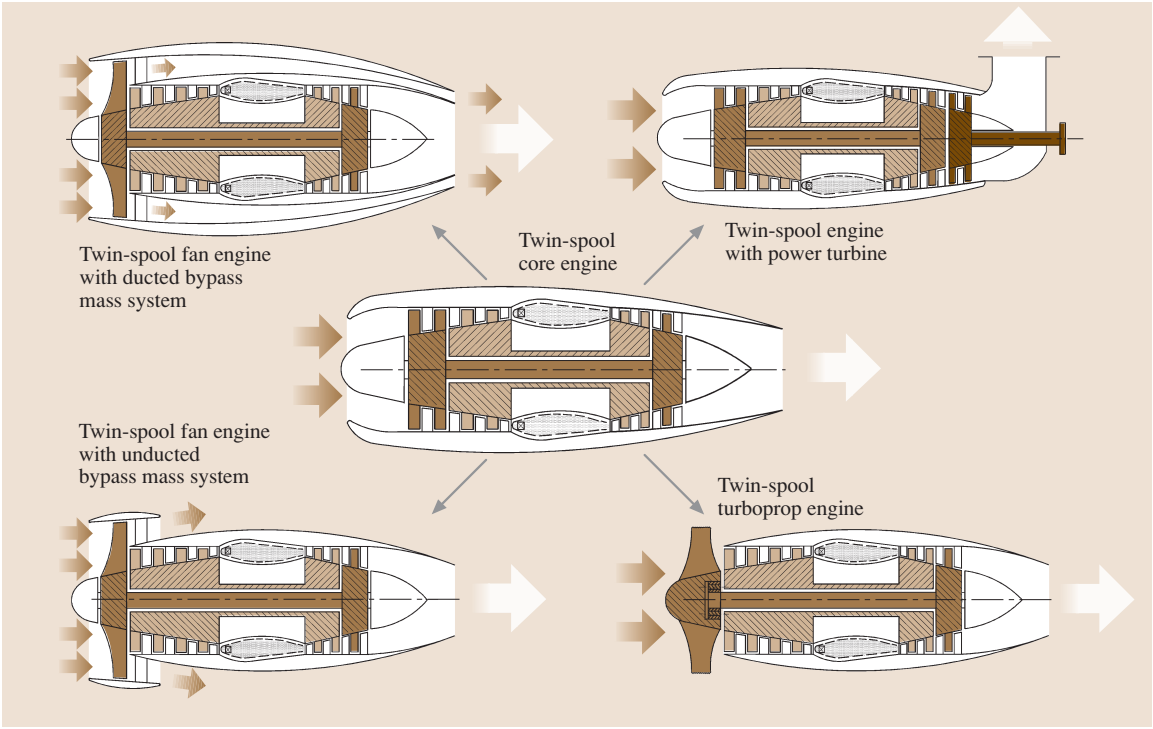


**Fig. 12.19** Schematic of a twin-spool core engine with its derivatives

mismatch between the turbine and compressor power that changes the spool rotational speed. This dynamic mismatch is brought to an equilibrium by taking appropriate control measures, as discussed in the following sections. As mentioned briefly, small gas turbines may have a split shaft configuration, as shown in Fig. 12.21. The single-spool gas generator unit provides the power turbine with combustion gas that has the required pressure and temperature to produce the power. As seen in Fig. 12.21a, the specific turbine enthalpy difference is $\Delta h_T \approx \Delta h_C$, leaving the remaining enthalpy difference $\Delta h_{PT}$ for power generation.

Figure 12.21b shows the $h$–$s$ diagram of a high-efficiency power generation gas turbine. The schematic cross section of this gas turbine is shown in Fig. 12.25. It consists of a multistage compressor C and a combustion chamber CC1, providing a lean combustion gas that expands in a single-stage reheat turbine (RT). The exhaust gas from the RT enters the second combustion chamber CC2, where the remaining fuel is added to ensure a stoichiometric combustion. It expands in the multistage turbine, which produces the major portion of power. As seen in the following sections, the implementation of the reheat process substantially increases the thermal efficiency of gas turbines. The underlying thermodynamic principles of this concept is the reheat process, which has been very well known in steam turbine design for more than a century. However, in gas turbine design, adding a second combustion chamber to a conventionally designed gas turbine seemed to be associated with unforeseeable problems. Based on design experiences with *compressed air energy storage* (CAES) gas turbines with two combustion chambers, *Brown Boveri* designed and successfully manufactured the first series of power generation gas turbines with a reheat stage and two combustion chambers.

### Gas Turbine Process

Accurate prediction of the thermal efficiency of a gas turbine engine requires knowledge of the compressor, combustion chamber, and turbine efficiencies as well as the bearing losses and the losses in auxiliary systems. Furthermore, detailed knowledge of the amount of mass flows with their extraction and injection pressures for cooling the turbine blades and the rotor discs are necessary. In addition, a detailed gas table that accounts for thermodynamic properties of humid air as well as the properties of the combustion gas must be implemented

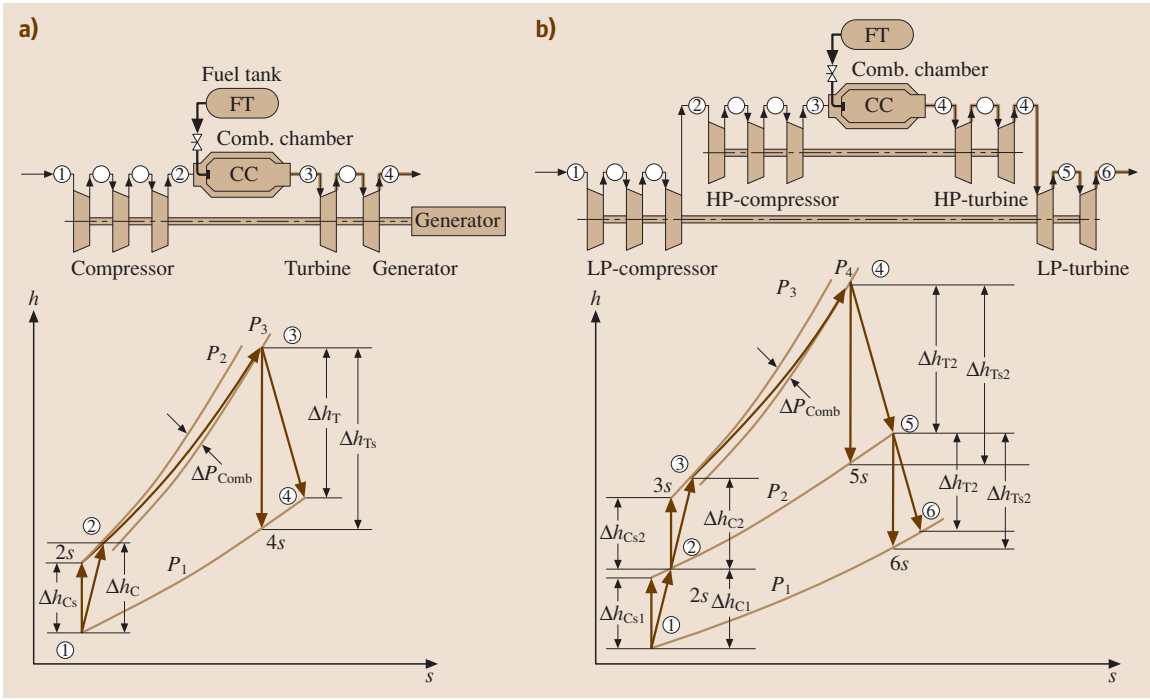


**Fig. 12.20a,b** *h–s* diagram of **(a)** a single-spool power generation gas turbine and **(b)** a twin-spool aircraft engine

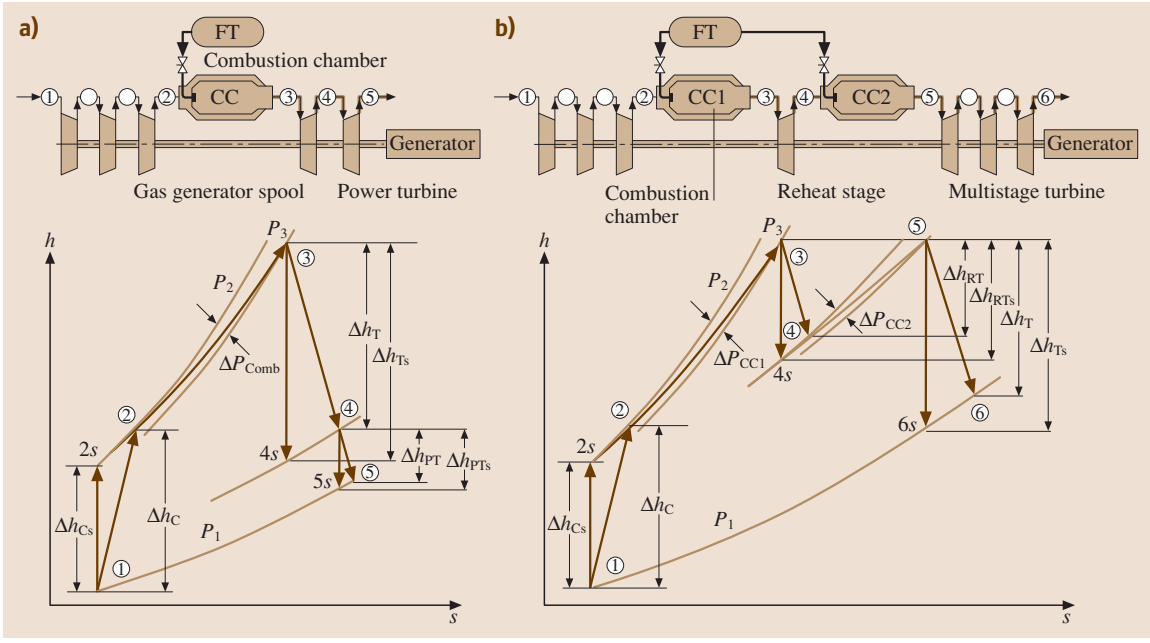


**Fig. 12.21a,b** *h–s* diagram of **(a)** a single-spool power generation gas turbine with a power shaft and **(b)** a single-spool power generation gas turbine with a reheat stage and two combustion chambers

into the calculation procedure. Assuming that air and combustion gas are calorically perfect gases results in significant errors. Figure 12.22 exhibits a schematic diagram that shows in detail the extraction of different cooling mass flows and their injection locations.

Mass flow through P1 extracted from plenum 3 cools the rotor and does not participate in power generation; mass flows through P2 and P3 cool the second and first turbine stages and remain in the system; and finally, mass flow through P4 reduces the combustion chamber exit temperature before it enters the turbine. At stations 6–8 and 11 humid air is mixed with combustion gas resulting in a local change of water-to-air and fuel-to-air ratios, therefore changing the entire thermodynamic properties including the special gas constant $R$. In the absence of the above information, reasonable assumptions relative to component efficiencies can be made to qualitatively determine the thermal efficiency and its tendency with regard to parameter variation. In the following section, a simple thermal efficiency calculation procedure is derived that is appropriate for varying different parameters and qualitatively determining their impacts on thermal efficiency.

The gas turbine with its corresponding process is sketched in Fig. 12.23. It consists of a compressor, a recuperator, a combustion chamber, and a turbine. Exhaust gas from the turbine is diverted into the recuperator, heating up the compressed air before entering the combustion chamber. The individual processes are compression, expansion, fuel addition and combustion, and heat exchange in the recuperator. The compressor and turbine enthalpy differences are calculated from

$$h_2 - h_1 = \frac{h_{2s} - h_1}{\eta_c} ,$$
$$h_3 - h_4 = (h_3 - h_{4s})\eta_T . \qquad (12.61)$$

We introduce the following definitions for the recuperator air and gas side (RA, RG), as well as combustion chamber (CC) pressure loss coefficients

$$\zeta_{RA} = \frac{\Delta P_{RA}}{P_2} , \text{ with } \Delta P_{RA} = P_2 - P_5 ,$$
$$\zeta_{RG} = \frac{\Delta P_{RG}}{P_1} , \text{ with } \Delta P_{RG} = P_4 - P_6 ,$$
$$\zeta_{CC} = \frac{\Delta P_{CC}}{P_2} , \text{ with } \Delta P_{CC} = P_5 - P_3 . \qquad (12.62)$$

The thermal efficiency is defined as

$$\eta_{in} = \frac{L_{net}}{\dot{Q}_{in}} = \frac{L_T - L_C}{\dot{Q}_{in}} = \frac{\dot{m}_T l_T - \dot{m}_C l_C}{\dot{Q}_{in}} . \qquad (12.63)$$

The specific net power is calculated from

$$\frac{L_{net}}{\dot{m}_1} = \frac{L_T - L_c}{\dot{m}_1} = \frac{\dot{m}_3 l_T - m_1 l_C}{\dot{m}_1} = (1+\beta) l_T - l_c , \qquad (12.64)$$

with the fuel air ratio $\beta = \dot{m}_f / \dot{m}_1$. Replacing the specific turbine power $l_T$ by the enthalpy difference from

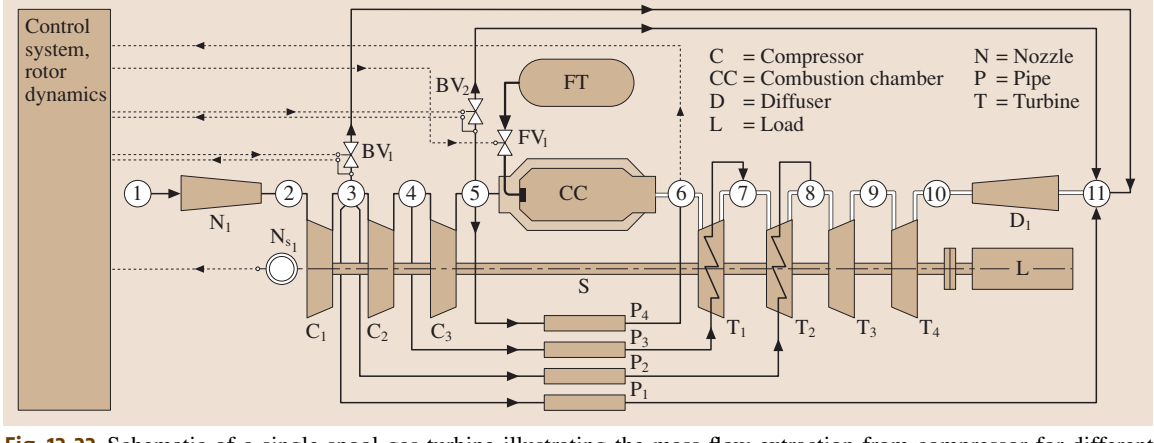


**Fig. 12.22** Schematic of a single-spool gas turbine illustrating the mass flow extraction from compressor for different cooling purposes

(12.61), we find

$$\frac{\dot{m}_3}{\dot{m}_1} l_T = (1+\beta)(h_3 - h_4) = \eta_T (1+\beta)(h_3 - h_{4s}) ,$$
$$\frac{\dot{m}_3}{\dot{m}_1} l_T = \eta_T (1+\beta)\bar{c}_{PT}(T_3 - T_{4s}) ,$$
$$\frac{\dot{m}_3}{\dot{m}_1} l_T = \eta_T (1+\beta)\bar{c}_{PT} T_3 \left(1 - \frac{T_{4s}}{T_3}\right) . \qquad (12.65)$$

Equation (12.65) expresses the isentropic enthalpy difference in terms of a product of averaged specific heat at constant pressure and the isentropic temperature difference. The specific heat in (12.65) exhibits an averaged value between the two given temperatures

$$\bar{c}_{PT} = \frac{h_3 - h_{4s}}{T_3 - T_{4s}} . \qquad (12.66)$$

The temperature ratio in (12.65) can be related to the pressure ratio by

$$\frac{T_3}{T_{4s}} = \left(\frac{p_3}{p_4}\right)^{\left(\frac{k-1}{k}\right)_T} = \pi_T^{\left(\frac{k-1}{k}\right)_T} = \pi_T^{m_T} ,$$
$$\text{with } m_T \equiv \left(\frac{k-1}{k}\right)_T . \qquad (12.67)$$

With (12.67), (12.65) becomes

$$\frac{\dot{m}_3}{\dot{m}_1} l_T = \eta_T (1+\beta)\bar{c}_{PT} T_3 \left(1 - \pi_T^{-m_T}\right) . \qquad (12.68)$$

Because of the pressure losses across the combustion chamber, the turbine and compressor pressure ratios are not the same ($\pi_T \neq \pi_c$). Implementing the pressure losses of the combustion chamber and recuperator air side, we find

$$\pi_T = \frac{p_3}{p_4} = \frac{p_2 - \Delta p_{RA} - \Delta p_{CC}}{p_1 + \Delta p_{RA}}$$
$$= \frac{p_2}{p_1}\left(\frac{1 - \zeta_{RA} - \zeta_{CC}}{1 + \zeta_{RA}}\right) = \pi_c \frac{1 - \zeta_{RA} - \zeta_{CC}}{1 + \zeta_{RA}} . \qquad (12.69)$$

We set the fraction on the right-hand side of (12.69) as

$$\epsilon = \frac{1 - \zeta_{RA} - \zeta_{CC}}{1 + \zeta_{RA}} \qquad (12.70)$$

and arrive at

$$\pi_T = \epsilon \pi_c , \text{ for } \epsilon = 0, \zeta_{RA} = \zeta_{CC} = \zeta_{RA} = 0$$
$$\text{and for } \epsilon > 0 \; \zeta_{RA} \neq 0 , \; \zeta_{CC} \neq 0 . \qquad (12.71)$$

For parameter variation, the following values may be used: $\zeta_{RA} \simeq \zeta_{RG} = 2\text{–}8\%$ and $\zeta_{CC} \simeq 5\text{–}10\%$. Following exactly the same procedure defined by (12.64)–(12.71), we find the compressor specific work as

$$l_C = \frac{1}{\eta_C} \bar{c}_{Pc} T_1 \left(\pi_C^{m_C} - 1\right) , \text{ with } m_C = \left(\frac{k-1}{k}\right)_C . \qquad (12.72)$$

Inserting (12.68) and (12.72) into (12.64), we arrive at

$$\eta_{th} = \frac{\eta_T \bar{c}_{PT} T_3 \left[1 - (\epsilon \pi_c)^{-m_T}\right](1+\beta)}{\bar{c}_{PCC} T_1 \left[(1+\beta)\frac{T_3}{T_1} - \frac{T_5}{T_1}\right]}$$
$$- \frac{\frac{1}{\eta_c}\bar{c}_{Pc} T_1 \left(\pi_c^{m_c} - 1\right)}{\bar{c}_{PCC} T_1 \left[(1+\beta)\frac{T_3}{T_1} - \frac{T_5}{T_1}\right]} . \qquad (12.73)$$

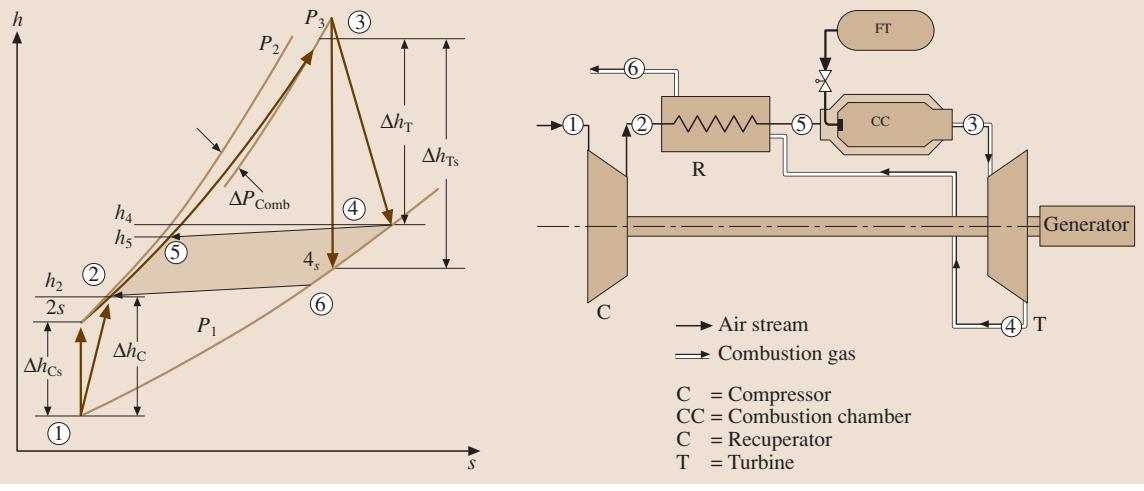


**Fig. 12.23** Simple sketch of a gas turbine with recuperator

The turbine inlet temperature $T_3$ and the environmental temperature $T_1$, and thus their ratio $T_3/T_1$, is considered as a known parameter. This parameter can also be used for parametric studies. Therefore it is desirable to express the ratio $T_5/T_1$ in terms of $T_3/T_1$. We find this ratio by utilizing the recuperator effectiveness $\eta_R$

$$\eta_R = \frac{h_5 - h_2}{h_4 - h_2} \simeq \frac{T_5 - T_2}{T_4 - T_2} \,. \tag{12.74}$$

From the compressor and turbine energy balance in (12.61) we find

$$\begin{aligned} T_2 &= T_1 + (T_{2s} - T_1)\frac{1}{\eta_c} = T_1 + T_1\left(\pi_c^{m_c} - 1\right)\frac{1}{\eta_c} \,, \\ T_4 &= T_3 - (T_3 - T_{4s})\eta_T = T_3 - T_3\left[1 - (\epsilon\pi_c)^{-m_T}\right]\eta_t \,. \end{aligned} \tag{12.75}$$

Equation (12.75) in dimensionless form yields

$$\begin{aligned} \frac{T_2}{T_1} &= 1 + \frac{1}{\eta_c}\left(\pi_c^{m_c} - 1\right) \,, \\ \frac{T_4}{T_1} &= \frac{T_3}{T_1} - \frac{T_3}{T_1}\eta_T\left[1 - (\epsilon\pi_c)^{-m_T}\right] \,. \end{aligned} \tag{12.76}$$

Introducing the temperature ratio $\theta = T_3/T_1$, the temperature ratio $T_4/T_1$ (12.76) becomes

$$\frac{T_4}{T_1} = \theta\left\{1 - \left[1 - (\epsilon\pi_c)^{-m_T}\right]\eta_T\right\} \,. \tag{12.77}$$

To determine the temperature ratio $T_5/T_1$, we rearrange (12.74) to obtain

$$\frac{T_5}{T_1} = \eta_R\left(\frac{T_4}{T_1} - \frac{T_2}{T_1}\right) + \frac{T_2}{T_1} \,. \tag{12.78}$$

Using (12.76) and (12.77), (12.78) can be rearranged to

$$\begin{aligned} \frac{T_5}{T_1} = \eta_R\Bigg(&\theta\left\{1 - \left[1 - (\epsilon\pi_c)^{-m_T}\right]\epsilon_T\right\} - 1 \\ &- \frac{1}{\eta_c}\left(\pi_c^{m_c} - 1\right)\Bigg) + 1 + \frac{1}{\eta_c}\left(\pi_c^{m_c} - 1\right) \,. \end{aligned} \tag{12.79}$$

Introducing (12.79) and the definition $\theta = T_3/T_1$ into (12.73), the thermal efficiency equation for a gas turbine with a recuperator is written as

$$\begin{aligned} \eta_{th} = \Bigg(&\bar{c}_{PT}\eta_T\theta\left[1 - (\epsilon\pi_c)^{-m_T}\right](1 + \beta) \\ &- \frac{1}{\eta_c}\bar{c}_{Pc}\left(\pi_c^{m_c} - 1\right)\Bigg) \\ &\times\Bigg(\bar{c}_{PCC}\Big\{\theta(1 + \beta - \eta_R) \\ &- \left[1 + \frac{1}{\eta_c}\left(\pi_c^{m_c} - 1\right)\right](1 - \eta_R) \\ &+ \theta\eta_R\eta_T\left[1 - (\epsilon\pi_c)^{-m_T}\right]\Big\}\Bigg)^{-1} \,. \end{aligned} \tag{12.80}$$

From (12.80) special cases are obtained. Setting $\eta_R = 0$ gives the thermal efficiency of a gas turbine without recuperator. The ideal case the of Brayton cycle is obtained by setting all loss coefficients equal to zero, all efficiencies equal to unity, and $\bar{c}_{PC} = \bar{c}_{PCC} = c_{PT} = \text{const}$. Equation (12.80) properly reflects the effects of individual parameters on the thermal efficiency and can be used for preliminary parameter studies. As an example, Fig. 12.8 shows the effect of pressure ratio, the turbine inlet temperature, and the component efficiency on thermal efficiency for two different cases. As Fig. 12.24 shows, for each turbine inlet temperature, there is one optimum pressure ratio. For temperature ratios up to $\theta = 3.5$ pronounced efficiency maxima are visible within a limited $\pi$-range. When approaching higher inlet temperature, however, this range widens significantly.

For a gas turbine without recuperator, the thermal efficiency (the solid curves in Fig. 12.24) shows that, for $\theta = 4.0$, increasing the pressure ratio above 15 does not yield a noticeable efficiency increase. However, this requires the compressor to have one or two more stages. The temperature ratio $\theta = 4.0$ corresponds to a turbine inlet temperature of $T_3 = 1200\,\text{K}$ at a compressor inlet temperature of $T_1 = 300\,\text{K}$.

The dashed curves in Fig. 12.24 indicate that tangibly higher thermal efficiencies at a substantially lower pressure ratio can be achieved by utilizing recuperators. This is particularly advantageous for small gas turbines (so called *microturbines*) with power ranging from 50 to 200 kW. The required low maximum pressure ratio can easily be achieved by a single-stage centrifugal compressor. Comparing cases 1 and 2 in Fig. 12.24 shows that thermal efficiency reduces if low-efficiency components are applied.

### Improvement of Gas Turbine Thermal Efficiency

The above parameter study indicates that, for a conventional gas turbine with a near-optimum pressure ratio with or without a recuperator, the turbine inlet temperature is the parameter that determines the level of thermal efficiency. For small-size gas turbines, the recuperator is an inherent component of the gas turbine. For large power generation gas turbines, however, this is not a practical option. Using a recuperator in a large gas turbine requires a significantly lower pressure ratio, which results in a large-volume recuperator and turbine. As a result, in order to improve the thermal efficiency of conventional gas turbines, increasing the turbine inlet temperature seems to be the only option left. Considering this fact, in the past three decades,

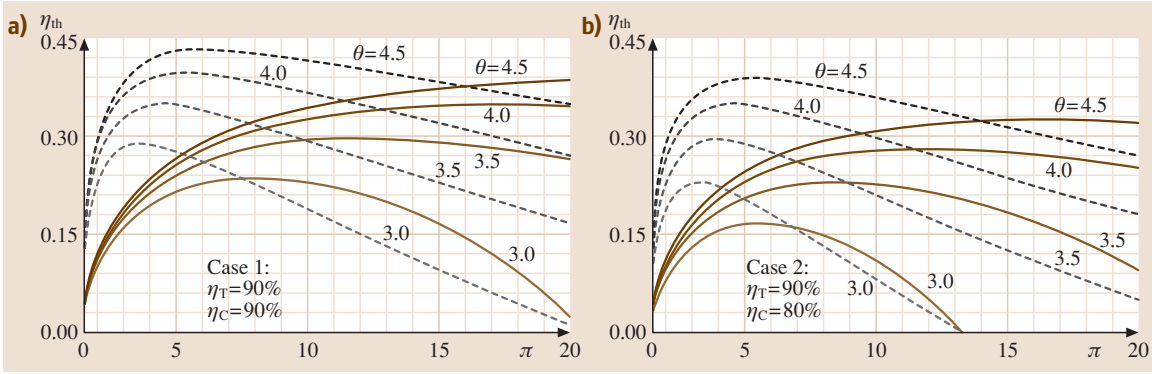


**Fig. 12.24a,b** Thermal efficiency as a function of pressure ratio with turbine inlet temperature ratio as a parameter for **(a)** a gas turbine with a recuperator (*dashed curves*) and **(b)** without a recuperator (*solid curves*). $\eta_R = 0.75$, $\zeta_{CC} = 0.05$, $\zeta_{RA} = \zeta_{RG} = 0.03$, for case 1 and case 2. In case 2 the turbine efficiency is lowered from 90% to 80%

gas turbine manufacturer have been concentrating their efforts on introducing more sophisticated cooling technologies, which are essential for increasing the turbine inlet temperature of conventional gas turbines.

To improve the thermal efficiency substantially without a significant increase in turbine inlet temperature, the well-known reheat principle as a classical method for thermal efficiency augmentation is applied. Although this standard efficiency improvement method is routinely applied in steam turbine power generation, it did not find its way into aircraft and the power generation gas turbine design. The reason for this was the inherent problem of integrating a second combustion chamber into a conventionally designed gas turbine engine. This issue raised a number of unforeseeable design integrity and operational reliability concerns. ABB (formerly Brown Boveri & Cie) was the first to develop a gas turbine engine with one reheat stage turbine followed by a second combustion chamber and a multistage turbine (Fig. 12.25).

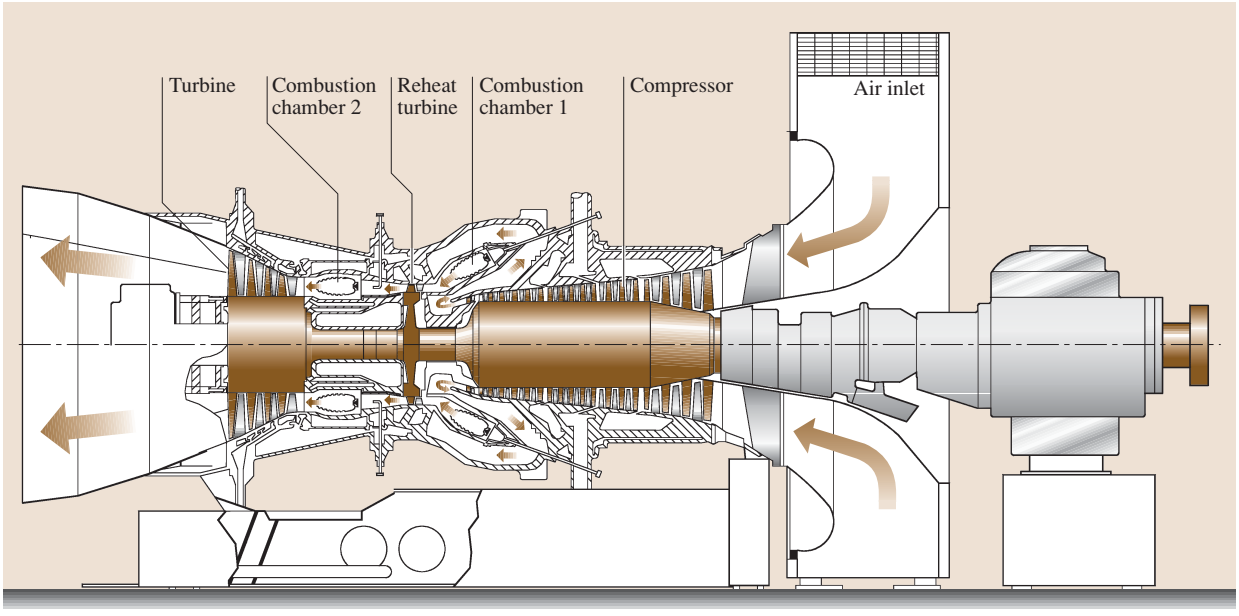


**Fig. 12.25** A schematic cross section of the GT-24 gas turbine engine with a single-stage reheat turbine and a second combustion chamber

A comparative study in [12.7] emulates, among others, two conceptually different power generation gas turbine designs utilizing components whose detailed aerodynamic performance characteristics were known. The first is a conventional gas turbine, whereas the second one has a reheat turbine stage and a second combustion chamber resembling the GT-24 [12.8]. Starting from a given environmental condition (pressure, temperature) and a consolidated turbine inlet temperature $T_{3BL} = 1200\,°C$ for both engines (Fig. 12.26a) the thermal efficiency is determined by the compressor pressure ratio and the compressor and turbine polytropic efficiencies $\eta_c$ and $\eta_T$ and is plotted in Fig. 12.27a. As curve 1 shows, for the given pressure ratio, which is not identical with the optimum pressure ratio, an efficiency of $\eta_{th} = 35\%$ is calculated. Substantial efficiency improvement is achieved by introducing a single-stage reheat principal, as applied to the GT-24. Details of the process are sketched in Fig. 12.26b with the baseline process as the reference process. The bright dotted area in Fig. 12.26b translates into the efficiency improvement, which in the case of the GT-24 resulted in efficiency improvement of 5.5% above the baseline efficiency. A detailed dynamic engine simulation of the GT-24 gas turbine engine with GETRAN© [12.9] verified a thermal efficiency of $\eta_{th} = 40.5\%$ plotted in Fig. 12.27a, curve 2. This tremendous efficiency improvement was achieved despite the facts that (a) the compressor pressure ratio is much higher than the optimal one for baseline engine and (b) the introduction of a second combustion chamber inherently causes additional total pressure losses. Further calculation showed that introducing a third combustion chamber would only result in a marginal improvement of 1–1.5% thermal efficiency, which does not justify the necessary research and development efforts to integrate a third combustion chamber. The specific work comparison is plotted in Fig. 12.27b, which shows a significant increase in specific work. Additional efficiency improvement requires a technology change. Major improvement can be achieved by using the ultrahigh-efficiency gas turbine (UHEGT) technology [12.8]. This technology eliminates the combustion chambers altogether and places the combustion process inside the stator blade passages (Sect. 12.2.6).

### 12.2.2 Nonlinear Gas Turbine Dynamic Simulation

The continuous improvement of efficiency and performance of aircraft and power generation gas turbine systems during the past decades has led to engine designs that are subject to extreme load conditions. The engine components operate near their aerodynamic, thermal, and mechanical stress limits. Under these circumstances, any adverse dynamic operation causes excessive aerodynamic, thermal, and subsequent mechanical stresses that may affect the engine safety, and reliability if adequate precautionary actions are not taken. Considering these facts, an accurate predic-

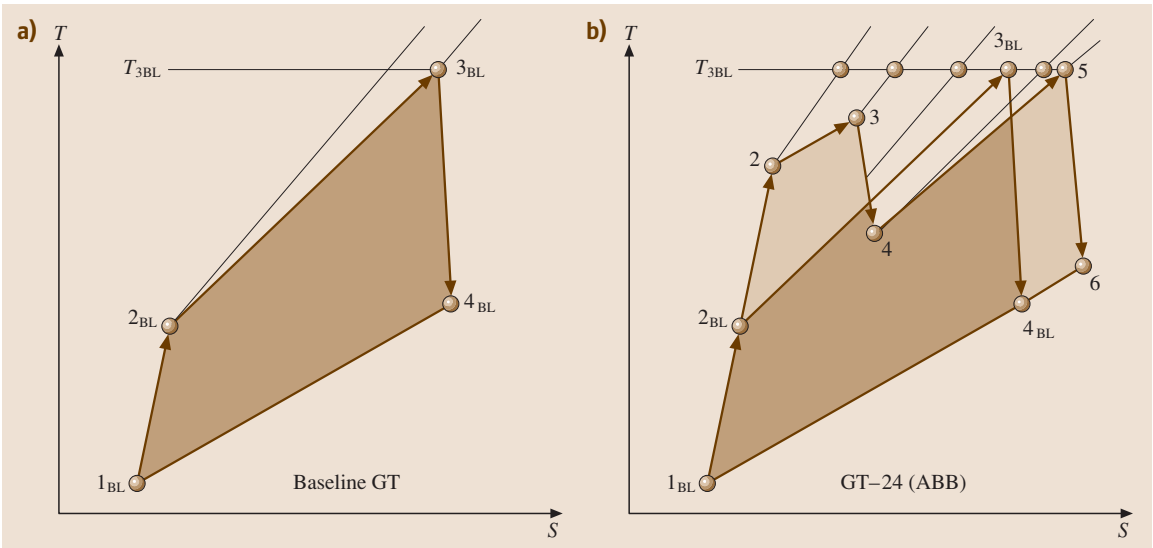


**Fig. 12.26a,b** Comparison of (a) a conventional baseline gas turbine process (b) with the GT-24 process after [12.7]

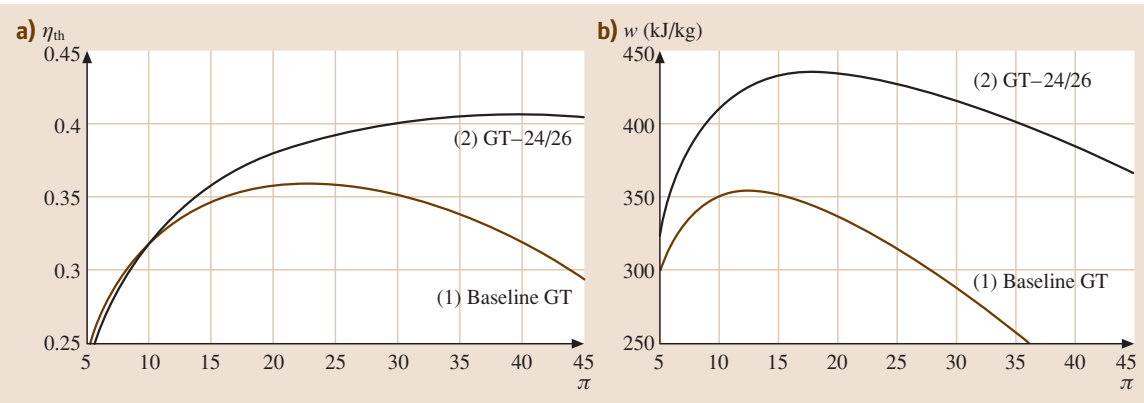


**Fig. 12.27a,b** Comparison of efficiency and specific work between a conventional baseline gas turbine and GT-24: **(a)** efficiency, **(b)** specific work

tion of the above stresses and their cause is critical at the early stages of design and development of the engine and its components. This section focuses on the simulation of the dynamic behavior of gas turbine engines and their components. The simulation spectrum encompasses single- and multispool gas turbine engines, turbofan engines, and power generation gas turbine engines. The simulation concept is based on a generic modularly structured system configurations. This concept is discussed in detail in [12.6], where the gas turbine components are represented by individual modules described mathematically by systems of differential equations. Based on these and other necessary modules, a generic concept is presented that provides the reader with necessary tools for developing computer codes for simulation of arbitrary engine and plant configurations ranging from single-spool thrust generation to multispool thrust/power generation engines under adverse dynamic operating conditions. It can easily be extended to rocket engines, combined cycles, cogeneration cycles, and steam power plants. In [12.6] a multilevel system simulation treats different degrees of complexity ranging from global adiabatic simulation to a detailed diabatic one. The dynamic behavior of the subject engine is calculated by solving a number of systems of partial differential equations which describe the unsteady behavior of the individual components. Accurate prediction of the dynamic behavior of the engine and the identification of critical parameters by using the method enables the engine designer to take appropriate steps using advanced control systems. The method may also be used to proof the design concept of the new generation of high-performance engines. The modular structure of the concept enables the user to independently develop new components and integrate them into the simulation code. As representative examples, four different case studies are presented that deal with dynamic simulation of a compressed air energy storage gas turbine, different transient cases with single- and multispool thrust, and power generation engines were simulated. The transient cases range from operating with a prescribed fuel schedule, to extreme load changes and generator shut down.

### 12.2.3 Engine Components, Modular Concept, and Module Identification

A schematic component arrangement and modeling of a twin-spool core engine is shown in Fig. 12.28. The corresponding modules are implemented into the engine modular configuration schematic in Fig. 12.29. Figures 12.30 and 12.31 show the lists of components with their corresponding modular representations and symbols that are described by the method presented in [12.6]. They exhibit the basic components essential for generically configuring any possible aero- and power generation gas turbine engines. These modules are connected with each other with a plenum, which is a coupling component between two or more successive components. As briefly explained in [12.6], the primary function of the plenum is to couple the dynamic information of entering and exiting components such as mass flow, total pressure, total temperature, fuel-to-air ratio, and water-to-air ratio. After entering the plenum a mixing process takes place, where the aforementioned quantities reach their equilibrium values. These values are the same for all outlet components.

A survey of power and thrust generation gas turbine engines has led to the practical conclusion that any arbitrary aircraft or power generation gas turbine engine and its derivatives, regardless of configuration, i. e., number of spools and components, can be generically simulated by arranging the components according to the engine configuration of interest. The nonlinear dynamic method presented in [12.6] is based on this generic, modularly structured concept that simulates the transient behavior of existing and new engines and their derivatives. The modules are identified by their names, shaft number, and inlet and outlet plena. This information is vital for automatically generating the system of differential equations representing individual modules. Modules are then combined into a complete system which corresponds to the engine configuration. Each module is physically described by the conservation laws of thermo-fluid mechanics which result in a system of nonlinear partial differential or algebraic equations. Since an engine consists of a number of components, its modular arrangement leads to a system containing a number of sets of equations. The above concept can be systematically applied to any aircraft or power generation gas turbine engine.

The general application of the modular concept is illustrated in Figs. 12.28 and 12.29. The twin-spool engine shown in Fig. 12.28 exemplifies the modular extension of the single-spool base engine. It consists of two spools with shafts $S_1$ and $S_2$, on which the low- and high-pressure components such as compressors and turbines are assembled. The two shafts are coupled by the working media air and combustion gas. They rotate with different speeds, which are transferred to the control system by the sensors $Ns_1$ and $Ns_2$. Air enters the inlet diffuser $D_1$, which is connected with the multistage compressor assembled on $S_1$, and is decomposed in several compressor stages $C_{1i}$. The first index (1) refers to the spool number and the second index $i$ marks the number of the compressor stage. After compression in the $S_1$ compressor stage group, the air enters the second compressor (HP compressor) assembled on the $S_2$ shaft, which consists of stages $C_{21}$–$C_{25}$. In the combustion chamber ($CC_1$) high-temperature combustion gas is produced by adding the fuel from the tank FT. The gas expands in the high-pressure turbine that consists of stages $T_{21}$–$T_{23}$. When exiting from the last stage of the HP turbine, the combustion gas enters the low-pressure turbine, consisting of stages $T_{11}$–$T_{13}$ and is expanded

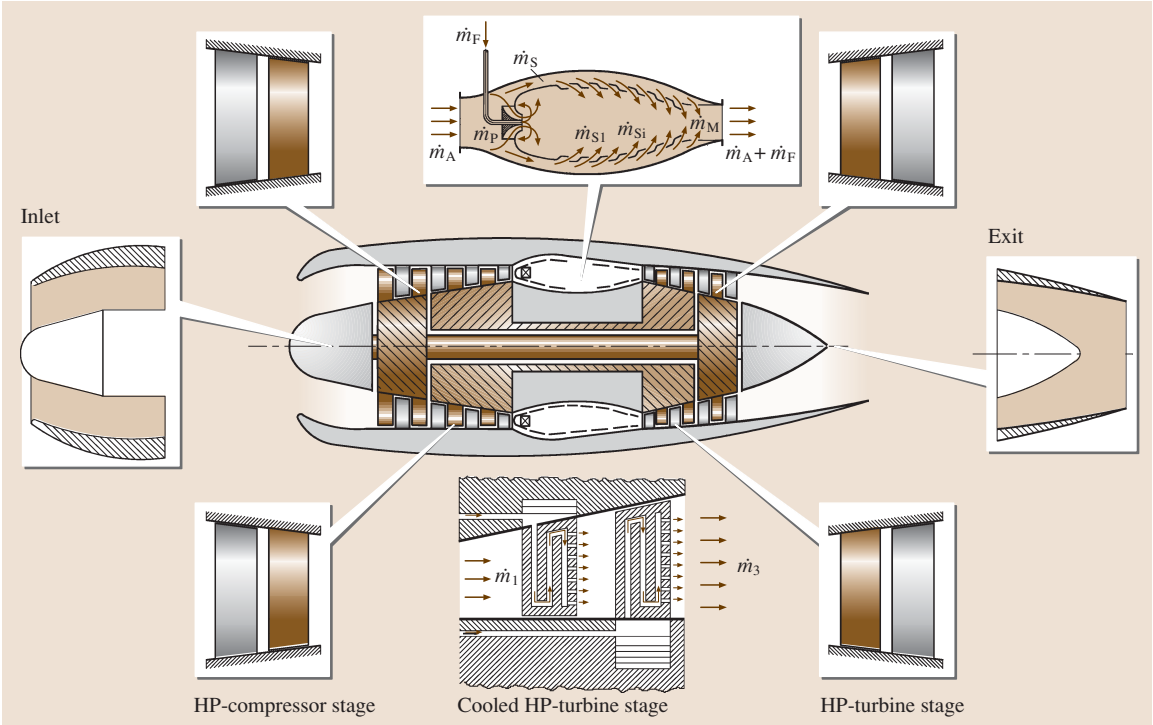


**Fig. 12.28** Schematic of a twin-spool core engine, component decomposition

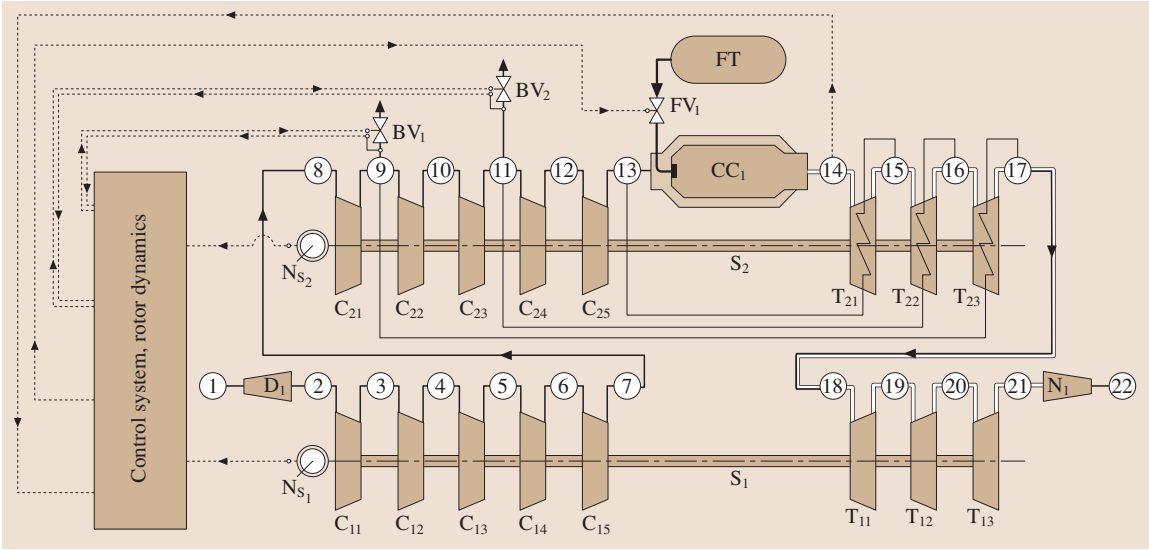


**Fig. 12.29** Modular configuration of the engine exhibited in Fig. 12.28

through the exit nozzle. Two bypass valves, $BV_1$ and $BV_2$, are connected with the compressor stator blades for surge prevention. The fuel valve, $FV_1$, is placed between the fuel tank, FT, and the combustion chamber, $CC_1$. The pipes, $P_i$, serve for cooling air transport from the compressor to cooled turbines. The compressor stage pressures, the turbine inlet temperature, and the rotor speed are the input signals to the control system, which controls the valve cross sections and the fuel mass flow.

Figure 12.32 shows a more complex example of a three-spool supersonic engine with its modular decomposition. Figure 12.33 exhibits a systematic modular configuration of Fig. 12.32 that is represented by a large system of differential and algebraic equations.

### 12.2.4 Levels of Gas Turbine Engine Simulations, Cross Coupling

The accuracy of gas turbine dynamic simulation is determined by the level of component modeling. It increases by increasing the level of simulation complexity. Four levels of simulation are introduced:

- The *zeroth simulation level* is applied to simple cases utilizing a fixed system configuration with steady-state component characteristics that are described by algebraic equations, simplified differential equations, and lookup tables and maps. Furthermore, there is no dynamic coupling between the components. Since this simulation level does not account for engine dynamics, it will not be discussed further.
- The *first simulation level* uses the component global performance map only for turbines and compressors. The maps are generated using the row-by-row adiabatic calculation method detailed in [12.6]. The other components such as recuperators, coolers, combustion chambers, pipes, nozzles, and diffusers are simulated according to methods discussed in [12.6]. Primary air, secondary combustion gas, and metal temperature of the combustion chamber are calculated. All modules are coupled with plena, ensuring a dynamic information transfer to all modules involved. Modules are described by algebraic and differential equations.
- The *second simulation level* utilizes adiabatic row-by-row or stage-by-stage calculation for the compressor and turbine modules. For combustion chamber, primary air, secondary combustion gas, and metal temperature are calculated. Dynamic calculations are performed throughout the simulation, where the modules are coupled by plena. Each module is described by differential and algebraic equations.
- The *third simulation level* uses diabatic row-by-row calculation for compressor and turbine modules. This level delivers very detailed diabatic information about the compressor and turbine component dynamic behavior. It utilizes cooled turbine and

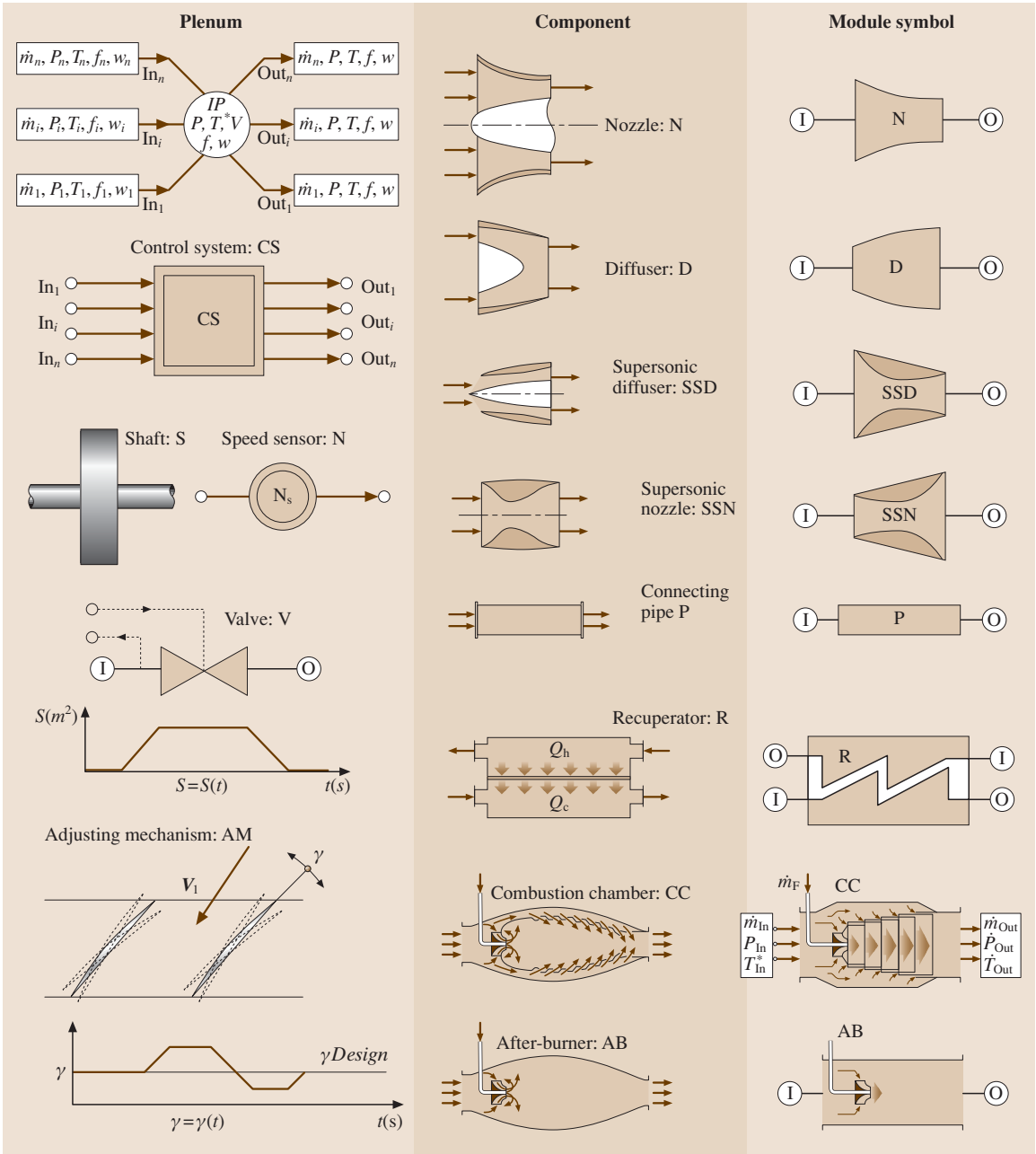


**Fig. 12.30** Components, modules, and their symbols: plenum, control system CS, shaft S, with moment of inertia $I$ and the rotational velocity $\omega$, speed sensor N, valve with an arbitrary ramp for closing and opening the cross section s, adjusting mechanism AM for stator blade adjustment, subsonic nozzle N, subsonic diffuser D, supersonic diffuser SSD, supersonic nozzle SSN, recuperator R, combustion chamber CC, and afterburner AB

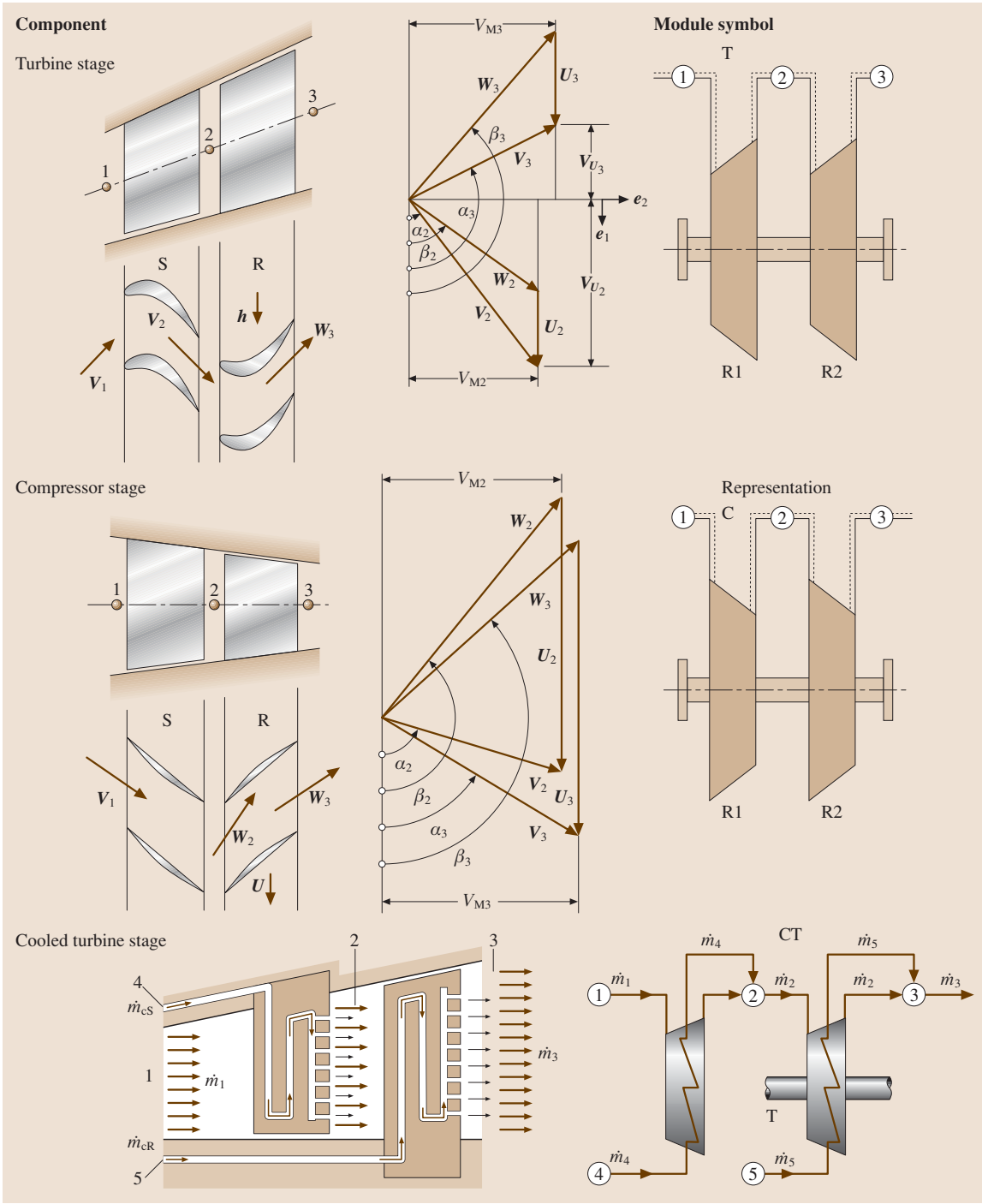


**Fig. 12.31** Adiabatic turbine stage with the module T, adiabatic compressor stage with the module C, cooled turbine stage with module CT

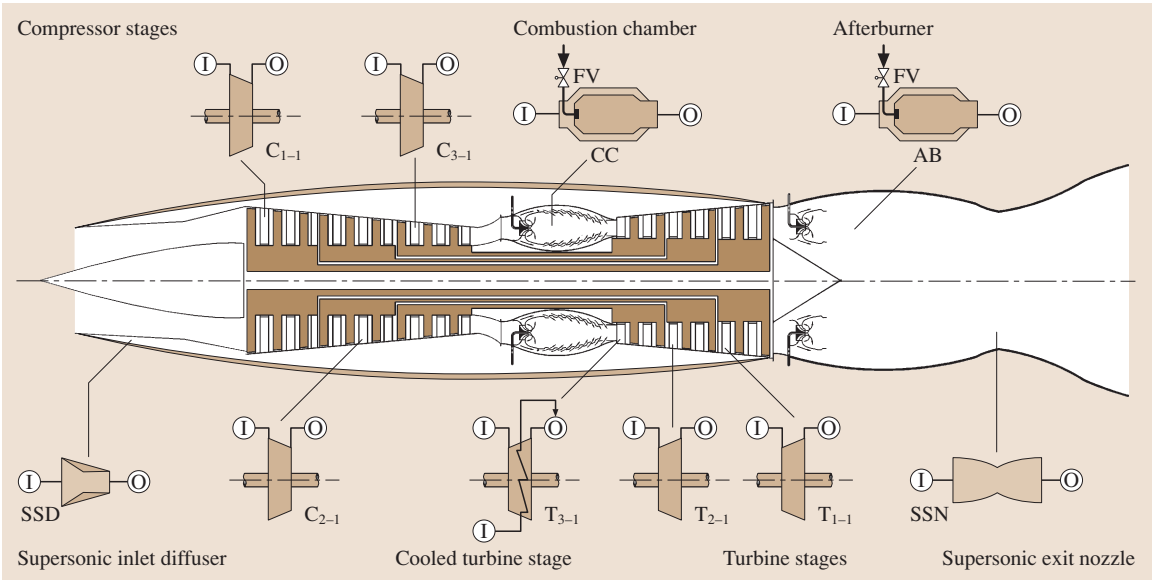


**Fig. 12.32** Schematic of a three-spool high-performance core engine, component decomposition

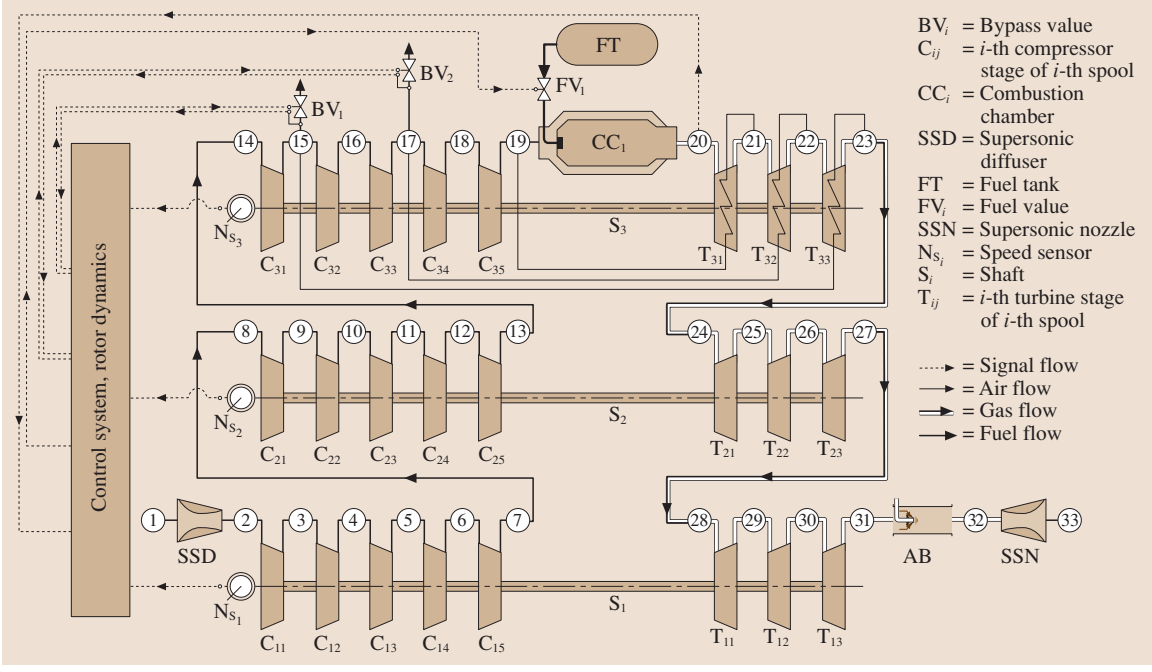


**Fig. 12.33** Modular configuration of the three-spool engine shown in Fig. 12.31. The three compressors and turbines are connected aerodynamically. The plena addressing, the spool number, and the component number uniquely identify the set of differential equations that describe the module

compressor stages and simultaneously calculates the blade temperatures. For the combustion chamber, primary air, secondary combustion gas, and metal temperature are calculated. Dynamic calculations are performed throughout the simulation, whereas the modules are coupled by plena. Each module is described by differential and algebraic equations. The details of information delivered by this level and degree of complexity is demonstrated by the following example. The first two stages of a four-stage turbine component of a high-performance gas turbine engine must be cooled. For the first four turbine rows we use the diabatic expansion process that requires three differential equations for describing the primary flow, three differential equations for describing the cooling flow, and one differential equation for describing the blade temperature. This leads from two cooled turbine stages to 28 differential equations.

The generic structure allows to cross-couple levels 1 to 3. For example, we wish to simulate a gas turbine engine with a global compressor performance map, but need to obtain detailed information about turbine blade temperature, which is necessary to calculate the relative expansion between the blades and the casing, then we may use the diabatic calculation method. In this case, we cross-couple the first- and third-level simulation.

### 12.2.5 Nonlinear Dynamic Simulation Case Studies

Three case studies dealing with three completely different gas turbine systems are presented. Table 12.1 shows the matrix of the cases where the engine types and transient-type simulations are listed. These studies demonstrate the capability of the generic structured method discussed in [12.6] to simulate complex systems dynamically and with high accuracy. The case studies presented in this chapter are related to real-world engine simulation and are intended to provide the reader with an insight into nonlinear engine dynamic simulation. The selected cases ranging from zero-spool, single-shaft power generation to three-spool four-shaft thrust and power generation gas turbine engines provide detailed information about the engine behavior during design and off-design dynamic operation. For each engine configuration the simulation provides aerothermodynamic details of each individual component and its interaction with the other system components. Since the presentation of the complete simulation results of the three cases listed in Table 12.1 would exceed the scope of this chapter, only a few selected plots will be displayed and discussed for each case.

#### Case Study 1: Compressed Air Energy Storage Gas Turbine

The subject of this case study is a zero-spool, single-shaft compressed air energy storage (CAES) gas turbine [12.1], which is utilized to cover peak electric energy efficiently demand during the day. Continuous increases of fuel costs have motivated the power generation industry to invest in technologies that result in fuel saving. Successful introduction of combined cycle gas turbines (CCGT) has drastically improved the thermal efficiency of steam power plants, which is equivalent to a significant fuel saving. Further saving is achieved by using the excess electrical energy available during the period of low electric energy demand (6–8 h during the night) to compress air into a large storage system. During periods of peak demand, the compressed air is injected into the combustion chambers and mixed with the fuel. After the ignition process is completed, the high-pressure high-temperature gas expands in the turbine, generating electric energy for about 2–4 h. In contrast to a CCGT, the period of operation of a CAES

**Table 12.1** Simulation case studies

| Tests | Gas turbine type | Transient type |
|---|---|---|
| Case 1 | CAES: Compressed air energy storage power generation gas turbine engine, zero-spool, single shaft, two turbines, two combustion chambers. | Generator and turbine shut down. |
| Case 2 | Single-spool, single-shaft, power generation gas turbine engine, BBCGT9. | Adverse load changes. |
| Case 3 | Three-pool, four-shaft, thrust and power generation core engine. | Operation with fuel schedule. |

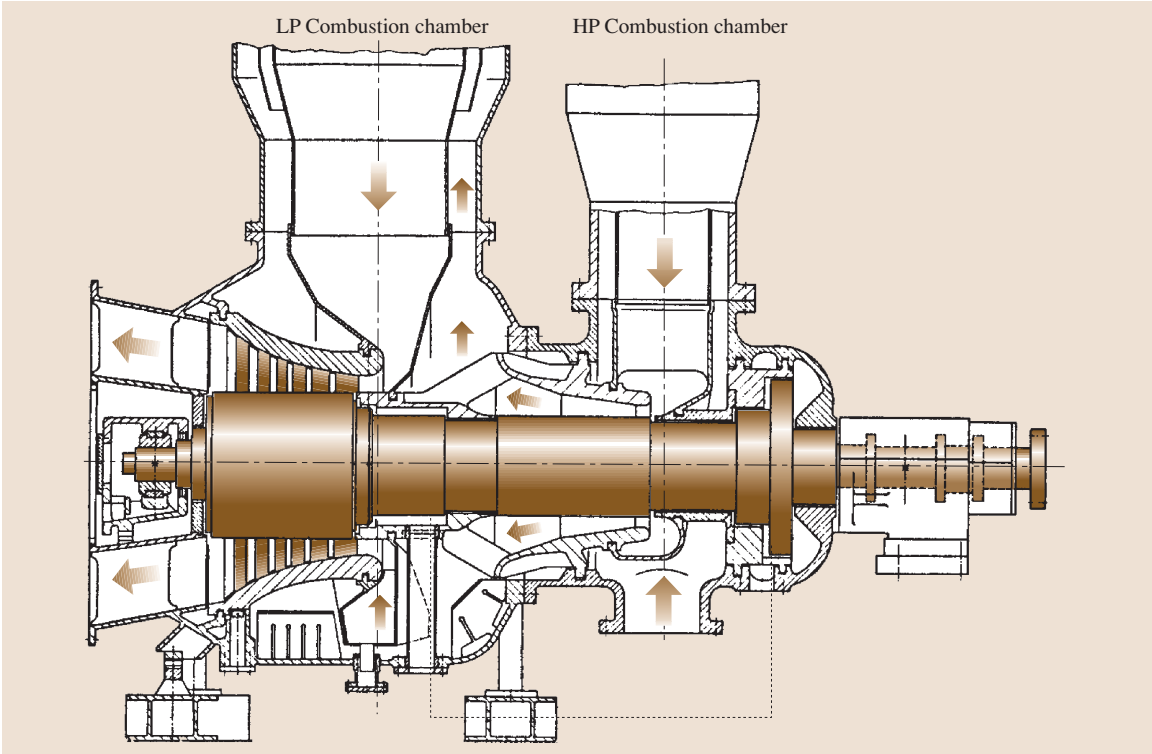


**Fig. 12.34** BBC-CAES-Huntorf gas turbine engine after [12.1]

plant is restricted to a few hours per day, resulting in a daily startup followed by a shutdown procedure. This relatively high frequency of startups and shutdowns may cause structural damages resulting in reduced lifetime if the startup and shutdown procedures are not performed properly. The condition for a safe startup procedure is outlined in this study, which helps the engine and control system designer to integrate this into their design procedure. The CAES gas turbine system (Fig. 12.34) with the simulation schematic shown in Fig. 12.35 features a large-volume plenum (8) for storing the compressed air, a high-pressure combustion chamber (HPCC), a high-pressure turbine (HPT), a low-pressure combustion chamber (LPCC), a low-pressure turbine (LPT2), a cold-air preheater with a low- and high-pressure side (LPP and HPP side) and a generator (G). During steady-state turbine operation, cold air from the air-storage facility, plenum 8, passes through the shutdown valve ($V_1$) to the inlet plenum (1), where it is divided into combustion and cooling-air flows. The addition of fuel in the HPCC causes the combustion air to be heated to the combustion chamber's exit temperature. Immediately upstream of the HPT, the combustor mass flow is mixed with a portion of the cooling-air flow, which has already been preheated in the HPP. As a result, the gas temperature of the turbine mass flow lies below the combustion chamber's exit temperature. After expansion in the HPT, the combustion chamber (LPCC) mass flow is mixed in the LPT inlet plenum (4) with the rest of the preheated cooling-air flow and the sealing-air flow. After expansion in the LPT, the gas gives off some of its heat in the LPP before leaving the gas turbine system.

Figure 12.35 shows how the various components are interconnected. Plenum 8, the air storage facility, is connected via two identical pipes (P6) to two shutdown valves ($V_1$). During steady-state operation, the blow-off valve ($V_2$) remains closed, being opened in the event of a disturbance likely to cause rapid shutdown. In such an event, the valve blows off some of the gas, thereby limiting the maximum rotor speed. For the sake of clarity, the preheater (P) has been separated into its air and gas sides, designated by HPP and LPP, respectively.

*Simulation of Emergency Shutdown.* Starting from a steady operating point, a generator trip with rapid

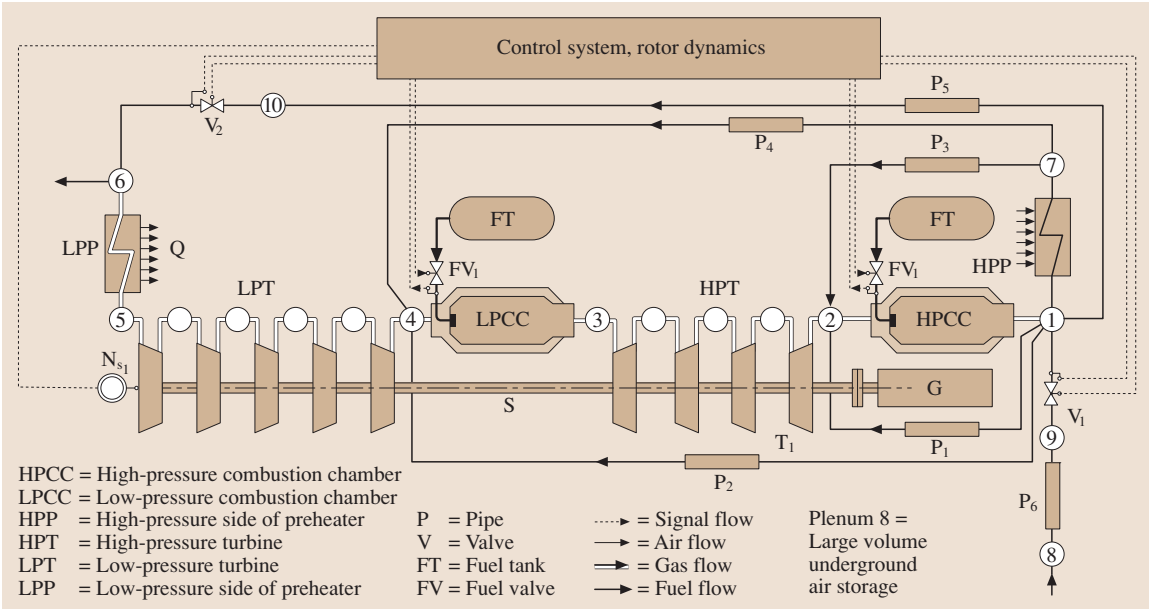


**Fig. 12.35** Simulation schematic of the CAES shown in Fig. 12.34

shutdown was simulated, assuming a failure of the control system. This circumstance necessitates an intervention by the hydraulic emergency system. This incident simulates an extreme transient process within some of the components, as explained briefly. After the generator trip, the rotor is strongly accelerated because of the full turbine power acting on it (Fig. 12.36a).

The hydraulic emergency system intervenes only when the speed corresponding to the hydraulic emergency overspeed trip is reached. This intervention involves closing the fuel valves, $FV_1$ and $FV_2$, and air valves $V_1$, after which the system no longer receives any energy from outside (Fig. 12.36b). It also involves opening the bypass/blow-off valve $V_2$, which allows the high-pressure air contained in both large-volume combustion chambers as well as in the HP side of preheater to discharge.

The closing process of the inlet and shutdown valves and the opening of the bypass valves are shown in Fig. 12.36b. This process results in a steady drop in plena pressures and temperatures. As Fig. 12.37 shows, the pressure drop in the high-pressure section is initially

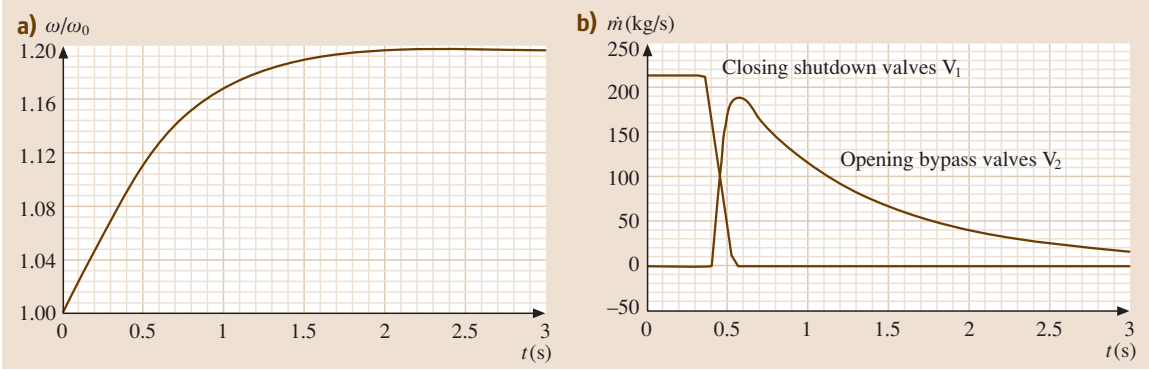


**Fig. 12.36** **(a)** Relative angular velocity **(b)** and mass flows as functions of time. The inlet shutdown valves $V_1$ remain open until the trip speed at $t = 0.35$ s has been reached. The same procedure is true for opening the blow-off valves $V_2$. Closing the shutdown valves follow the ramp shown in **(b)**

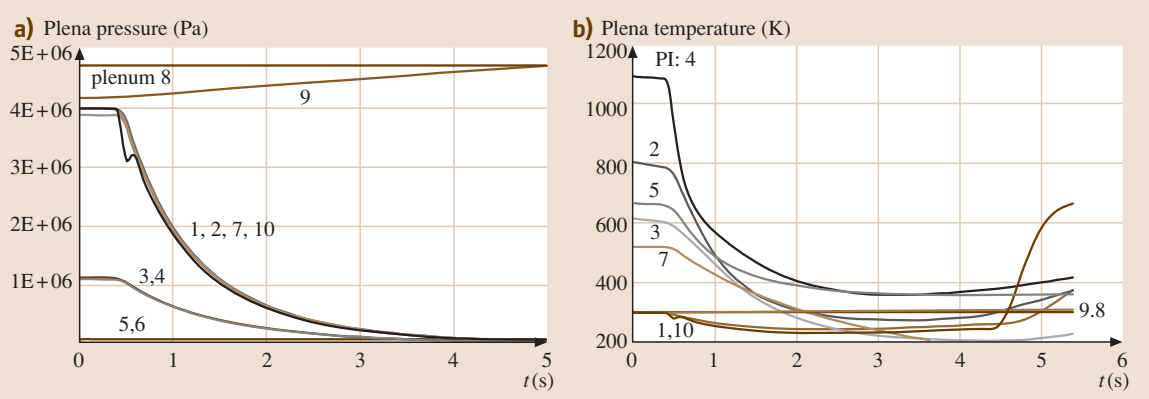


**Fig. 12.37** (a) Plena pressure and (b) temperature as functions of time. The shutdown process causes rapid depressurization in the high-pressure plena 1, 2, 7, and 10

steeper than in the low-pressure section. This means that the enthalpy difference of the high-pressure turbine is reduced more rapidly than that of the low-pressure turbine. Immediately after the blow-off valve is opened, an abrupt pressure drop takes place in plenum 10, which is connected to plenum 1 via pipe $P_5$. Thereafter, dynamic pressure equalization takes place between the two plena. This drop in pressure and temperature causes a corresponding drop in the shaft power and the mass flow throughout the engine. Figure 12.38 shows the resulting drop in turbine inlet and exit temperature. The continuous decrease in turbine mass flow causes a strong dissipation of shaft power, resulting in the excessive increase of turbine exit temperature. In order to avoid thermal damages to the blades, a small stream of cold air is injected into the turbine flow path, which causes a reduction in temperature gradient. This is shown in Fig. 12.38 for the exit temperature at $t = 3.4$ s.

Dynamic behavior of the rotor speed is generally determined by the turbine power acting on the rotor. How the rotor behaves in response to a generator trip depends, in particular, on how long the full turbine power is available, a process monitored by the control and safety monitoring system. When the control system functions normally, a trip is signaled without delay to the shutdown valve. Failure of the control system causes the hydraulic emergency system to intervene. The intervention begins only when the speed corresponding to the hydraulic emergency overspeed trip is reached. During this process, and also the subsequent valve dead time, the rotor receives the full turbine power. The closing phase is characterized by a steady reduction in energy input from outside, which finally becomes zero. The total energy of the gases still contained in the system is converted by the two turbines into mechanical energy, causing the rotor speed to increase steadily (Fig. 12.36). When the instantaneous turbine power is just capable of balancing the friction and ventilation losses, the rotor speed reaches its maximum, after which it begins to decrease. Reducing the turbine mass flow (Fig. 12.39a) below the minimum value discussed in [12.6] causes the shaft power to dissipate completely as heat, resulting in negative values, as shown in Fig. 12.39b. From this point on, the rotational speed starts to decrease. Figure 12.39a depicts the mass flows through the HP and LT turbines that generate the total shaft power (Fig. 12.39b).

### Case Study 2: Power Generation Gas Turbine Engine

The subject of this case study is the dynamic simulation of a BBC-GT9 gas turbine which is a single-spool single-shaft power generation gas turbine engine. It is utilized as a stand-alone power generator or in conjunction with combined cycle power generation. The engine shown in Fig. 12.40 consists mainly of three compressor stage groups, a combustion chamber, a turbine, a control system, and a generator.

The simulation schematic of this engine is presented in Fig. 12.41. The rotor speed and turbine inlet temperature are the input parameters for the controller, its output parameters are the fuel mass flow (fuel valve opening), and the mass flows of the bypass valves (bypass valve opening). The dynamic behavior of BBC-GT9 was experimentally determined for transient tests with extreme changes in its load. Its transient data was accurately documented by *Schobeiri* [12.9]. Starting from a given

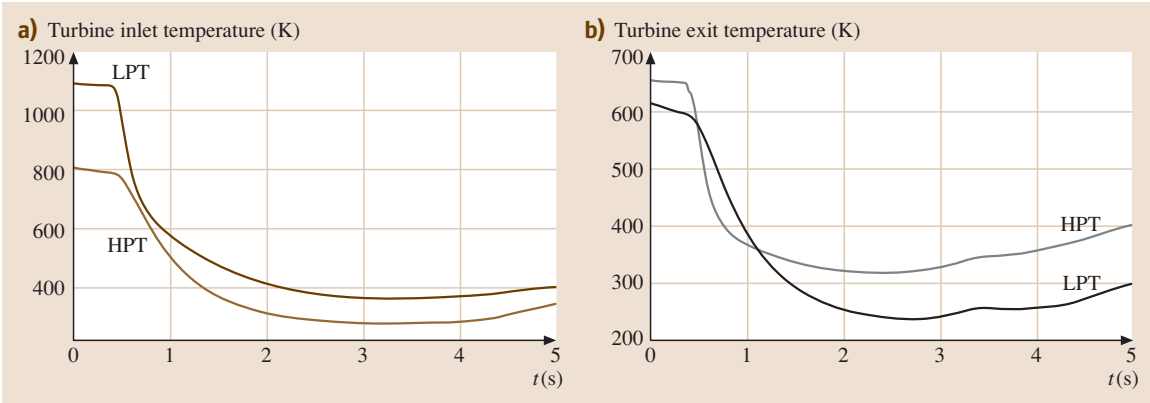


**Fig. 12.38** **(a)** Turbine inlet and **(b)** exit temperature as functions of time. Note the changes of the exit temperature at $t = 3.4\,\mathrm{s}$

network load schedule, the dynamic behavior of the gas turbine is predicted and the results are presented.

The engine under consideration consists mainly of three compressor stage groups, a combustion chamber, a turbine, a control system, and a generator. The simulation schematic of this engine is similar to that of Fig. 12.42. For dynamic simulation, the first, second, and third stage groups are simulated using the row-by-row technique [12.6]. A similar row-by-row calculation procedure is applied to the turbine component. The rotor speed and the turbine inlet temperature are the input parameters for the controller; its output parameters are the fuel mass flow (fuel valve opening) and the mass flows of the bypass valves (bypass valve opening).

*Simulation of an Adverse Dynamic Operation.* Starting from steady state, in accordance with the load schedule indicated in Fig. 12.42a (curve 1), after 1 s, a generator loss of load is simulated that lasts for 6 s. The rotor at first reacts with a corresponding increase in rotational speed (Fig. 12.42b), which results in a rapid closing of the fuel valve (Fig. 12.42b). The rotational speed is then brought to an idling point and held approximately constant. The process of control intervention lasts until a constant idling speed is attained. After that, there is an addition of load in sudden increases, such that the gas turbine is supplying approximately 25% of its rated load (Fig. 12.42). The rotor first reacts to this addition of load with a sharp decrease in rotational speed, as exhibited in Fig. 12.42, causing a quick opening of the fuel valve (Fig. 12.42). After completion of the transient process, the steady off-design state is reached.

*Plena Pressure and Temperature Transients.* The above adverse dynamic operation triggers temporal changes of the flow quantities within individual com-

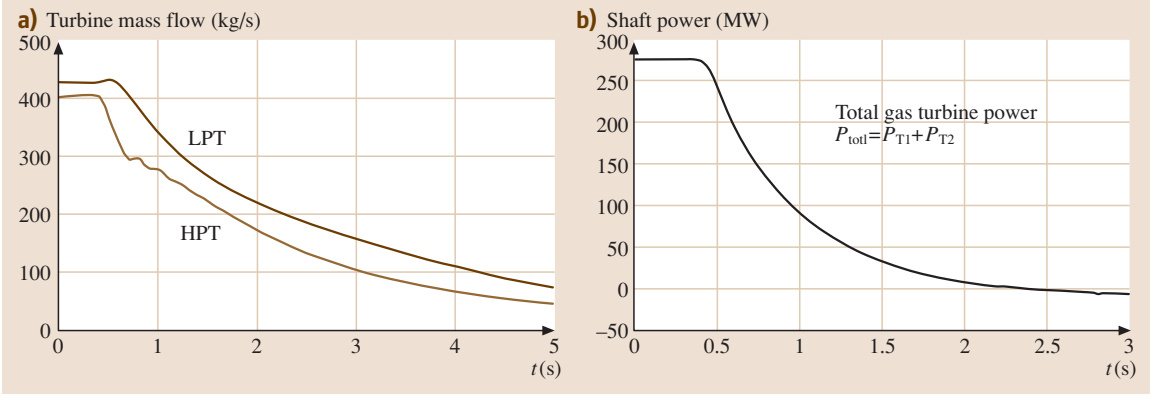


**Fig. 12.39** **(a)** Turbine mass flow and **(b)** shaft power as functions of time

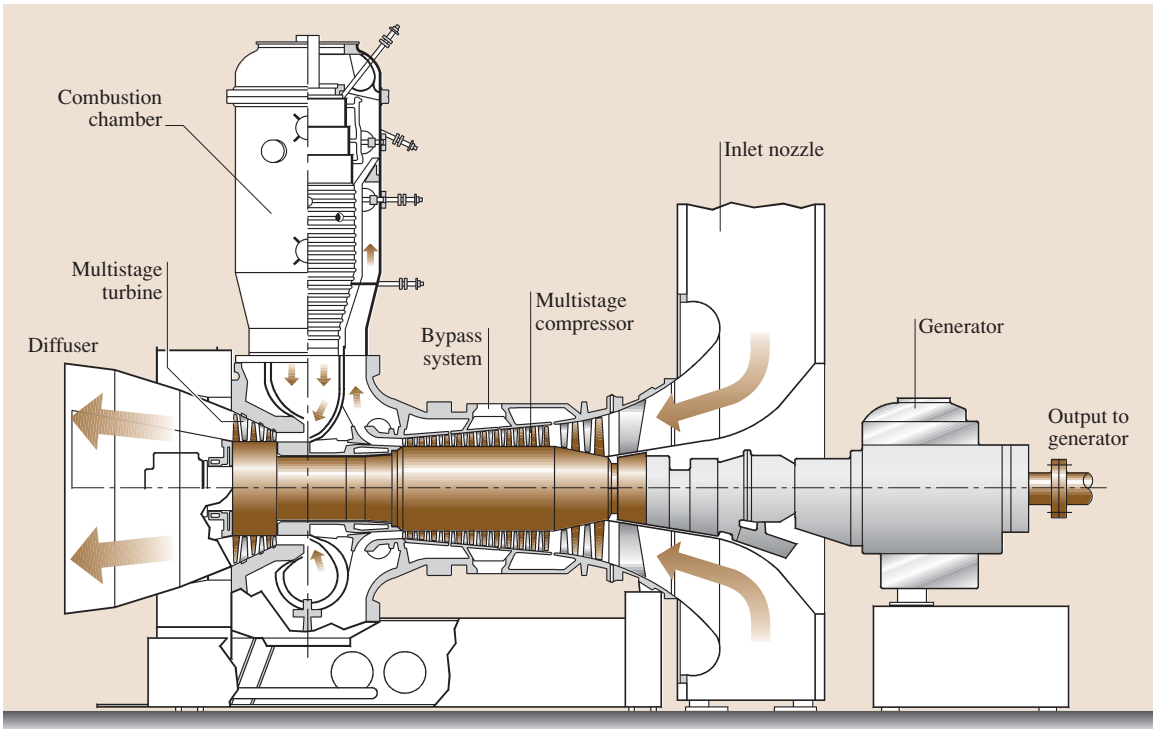


**Fig. 12.40** A single-spool power generation gas turbine BBC-GT9

ponents. Figure 12.43 shows how the plena pressure and temperature change with time. Decrease of turbine power and increase of the shaft speed (Fig. 12.42) has caused the HP compressor exit pressure in plenum 5 to decrease. The temperature at the combustion chamber exit, plenum 6, and turbine exit, plenum 7, follow the course of fuel injection shown in Fig. 12.47b. The plena temperature upstream of the combustion chamber are not affected.

*Compressor and Combustion Chamber Mass Flow Transients.* Figure 12.44 exhibits the mass flow transients through low pressure (LP), intermediate pressure (IP), and high pressure (HP) compressors. While the IP- and HP-stage groups have the same mass flow, the LP part has a greater mass flow. The difference of 1 kg/s is due to the cooling mass flow extraction. As briefly mentioned, the increase in shaft speed and the simultaneous decrease in compressor power consumption leading to

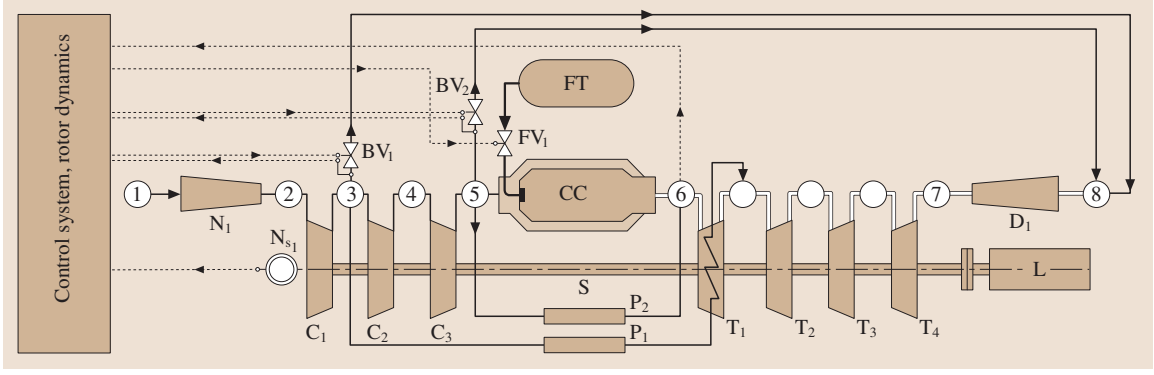


**Fig. 12.41** Simulation schematic of BBC-GT9 shown in Fig. 12.40

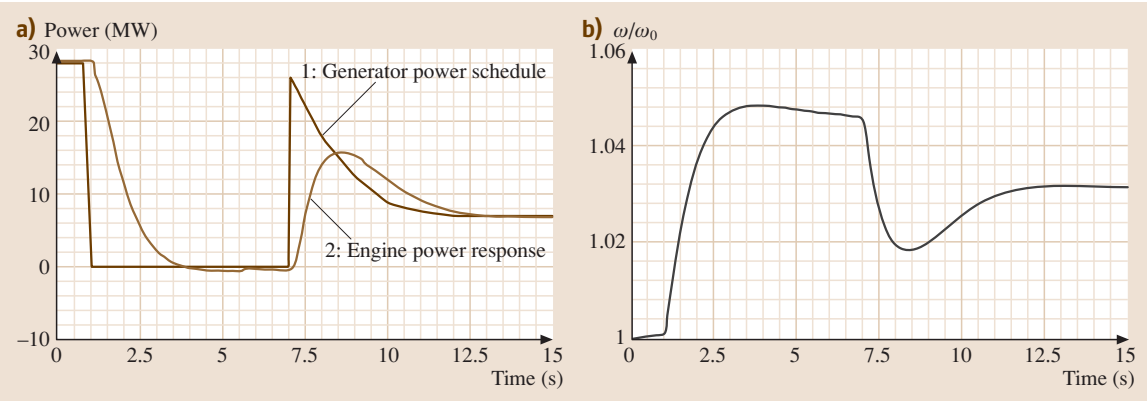


**Fig. 12.42** **(a)** Generator load schedule (*curve* 1). Sequence of events: steady operation from 0 to 1 s, sudden loss of load, idle operation, sudden addition of load, continuous decrease of load to 25%. *Curve* 2: engine power response. **(b)** Relative shaft speed as a function of time

the compressor pressure drop has caused an increase in the compressor mass flow during the process of loss of load that lasts up to $t = 6$ s. The sudden load addition reduces the compressor mass flow.

The combustion chamber mass flow shows a similar course with a substantial difference: a substantial portion of the compressor mass flow is extracted for combustion chamber exit temperature mixing cooling.

*Combustion Chamber Gas and Metal Temperature Transients.* The combustion chamber component used in this simulation has three segments that separate the primary combustion zone from the secondary cooling air zone. Its module is shown in Fig. 12.45. Figure 12.46 exhibits the combustion chamber gas and metal temperatures as functions of time. Compressed air enters the combustion chamber at station 1 (Fig. 12.46). Fuel is added and the segment cooling occurs according to the procedure described in [12.6]. The secondary mass flow portions $\dot{m}_{Si}$ serve as cooling jets and are mixed with the combustion gas, thus reducing the gas temperature. Before exiting, the combustion gas is mixed with the mixing air stream $\dot{m}_M$, further reducing the temperature. Figure 12.46b shows the mean segment temperatures. In accordance with the measurements on this gas turbine, the flame length extends from station 1 to 3, which makes segment number 2 the hottest one. We assumed that all secondary cooling channels are open.

*Turbine and Fuel Mass Flow Transients.* Figure 12.47a exhibits the turbine mass flow transient, which is dictated by the compressor dynamic operation. The difference between the turbine and the compressor mass flow is the injected fuel mass flow. The particular course

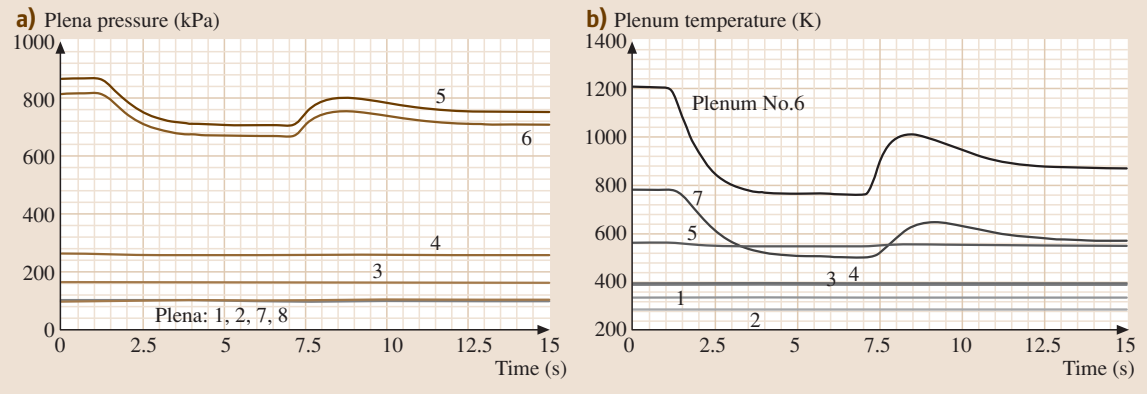


**Fig. 12.43** **(a)** Plena pressure and **(b)** temperature as functions of time. Individual plena are labeled

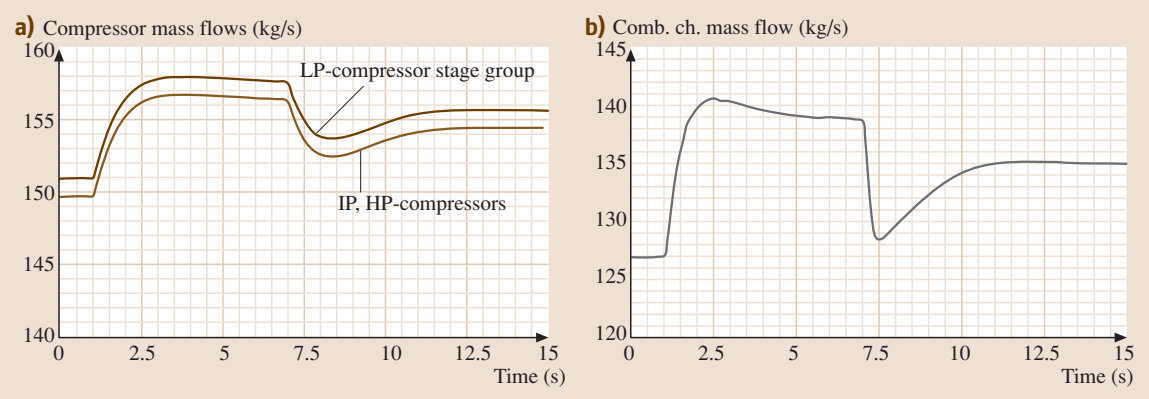


**Fig. 12.44** (a) Compressor and (b) combustion chamber mass flows as functions of time

of fuel mass flow shown in Fig. 12.47b is due to the intervention of the control system. An increase in rotational speed causes the controller to close the fuel valve. Subsequent addition of generator load results in a steep drop of rotational speed, which causes an opening of the fuel valve.

### Case Study 3: Simulation of a Multispool Gas Turbine Engine

The subject of this study is the nonlinear dynamic simulation of a gas turbine engine with a higher degree of complexity than the previous cases. For this purpose a three-spool thrust-generating gas turbine engine is designed that incorporates advanced components. The three-spool four-shaft high-performance gas turbine engine consists of a low-pressure spool that incorporates the LP compressor and turbine connected via shaft $S_1$. The intermediate pressure spool integrates the IP compressor and turbine connected via shaft $S_2$. The high-pressure spool carries the HP compressor and HP turbine on shaft $S_3$. To increase the level of engine complexity, a fourth shaft, $S_4$, with the power generating turbine $T_4$, was attached to the exit of the three-spool gas generating unit as shown in Fig. 12.48. The transient operation is controlled by a given fuel schedule. The component nomenclature for this configuration is the same as for the previous cases. The simulation schematics shown in Fig. 12.48 represents the modular configuration of the gas turbine.

*Fuel Schedule and Rotor Response.* The dynamic behavior of the above engine is simulated for an adverse acceleration–deceleration procedure (Fig. 12.49).

The transient operation is controlled by an open-loop fuel schedule shown in Fig. 12.49a. The three spools and the fourth shaft run independently at different rotational speed (Fig. 12.49b). The fuel schedule generated completely arbitrarily simulates an acceleration–deceleration procedure with emphasis on deceleration. We start with the steady-state operation and reduce the fuel mass flow to $\dot{m}_F = 2.8\,\mathrm{kg/s}$ for about 2 s. During this short period of time, the engine operates in a dynamic state which is followed by a cyclic acceleration–deceleration event with the ramps given in Fig. 12.49. The dynamic operation triggers a sequence of transient events within individual components that are discussed in the following sections.

*Rotor Speed Behavior.* The transient behavior of the three spools as well as the power shaft is determined by the net power acting on the corresponding rotor. For each individual spool, the cyclic acceleration–deceleration event has caused a dynamic mismatch between the required compressor power consump-

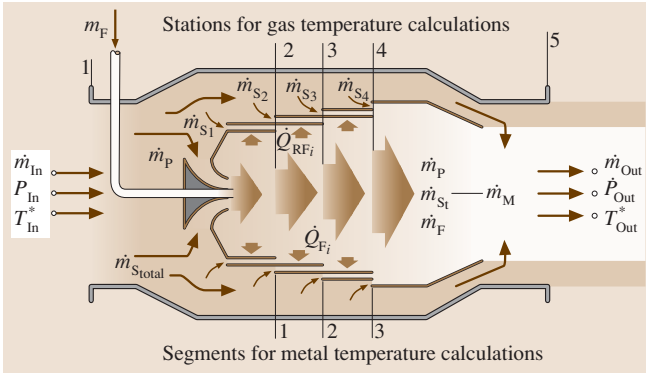


**Fig. 12.45** Combustion chamber module, stations and segments, $\dot{m}_P$ – primary $\dot{m}_{S_{tot}}$ – total secondary air, $\dot{m}_{Si}$ – individual secondary air

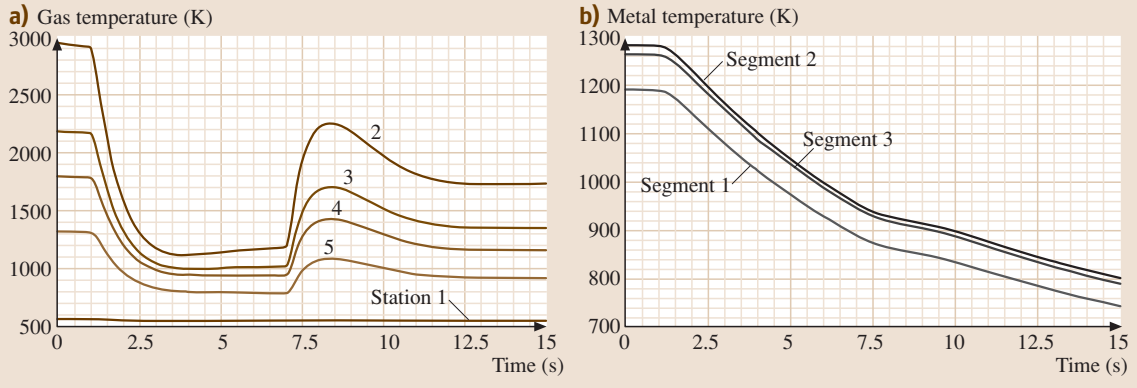


**Fig. 12.46** **(a)** Combustion chamber gas and **(b)** metal temperature at different positions as functions of time

tion and the turbine power generation, as shown in Fig. 12.50. While the LP and IP spools 2 and 3 decelerate under the influence of negative net power, the HP spool 3 reacts faster to the acceleration. Since the fuel schedule places special weight upon deceleration, the rotational speeds of all three spools have a decelerating tendency as shown in Fig. 12.50.

*Pressure and Temperature Transients within Plena.* The change in fuel mass flow triggers a chain of transient events within the plena, as shown in Fig. 12.51. Plena pressure 5 and 6, which corresponds to the exit pressure of the HP compressor and the combustion chamber, are strongly affected by the cyclic fuel change, whereas the other plena that correspond to the inlet and exit plena of the remaining components experience moderate changes. The plena temperature distributions downstream of the combustion chamber shown in Fig. 12.51b reflect the course of the fuel schedule.

*Combustion Chamber Gas and Metal Temperature Transients.* Figure 12.52 exhibits the combustion chamber gas and metal temperatures as functions of time. The combustion chamber component used in this simulation has three segments that separate the primary combustion zone from the secondary cooling air zone. Its module is shown in Fig. 12.47. Compressed air enters the combustion chamber at station 1 (Fig. 12.52a). Fuel is added and the segment's cooling occurs according to the procedure described in [12.6]. The secondary mass flow portions serve as cooling jets and are mixed with the combustion gas, thus reducing the gas temperature. Before exiting, the combustion gas is mixed with the mixing airstream, further reducing the temperature. Figure 12.52a shows the mean segment temperatures.

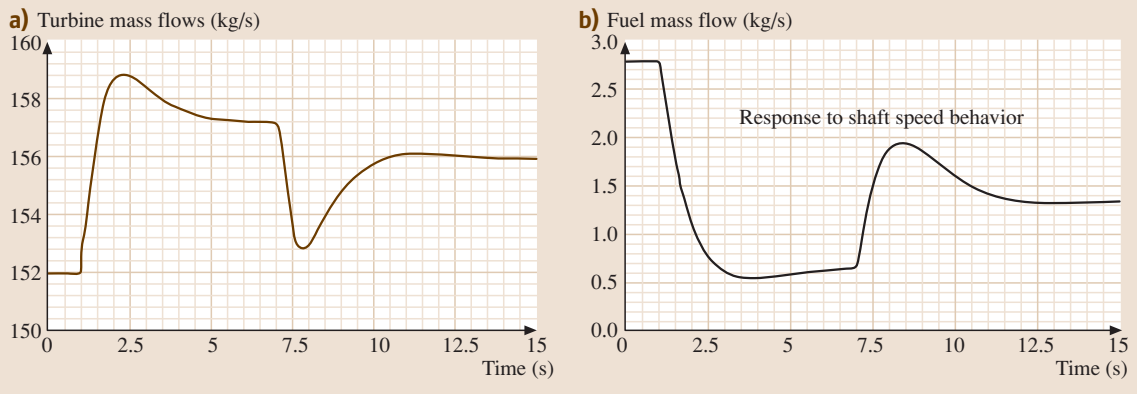


**Fig. 12.47** **(a)** Turbine and **(b)** fuel mass flow as functions of time. The fuel mass flow is controlled by the shaft rotational speed

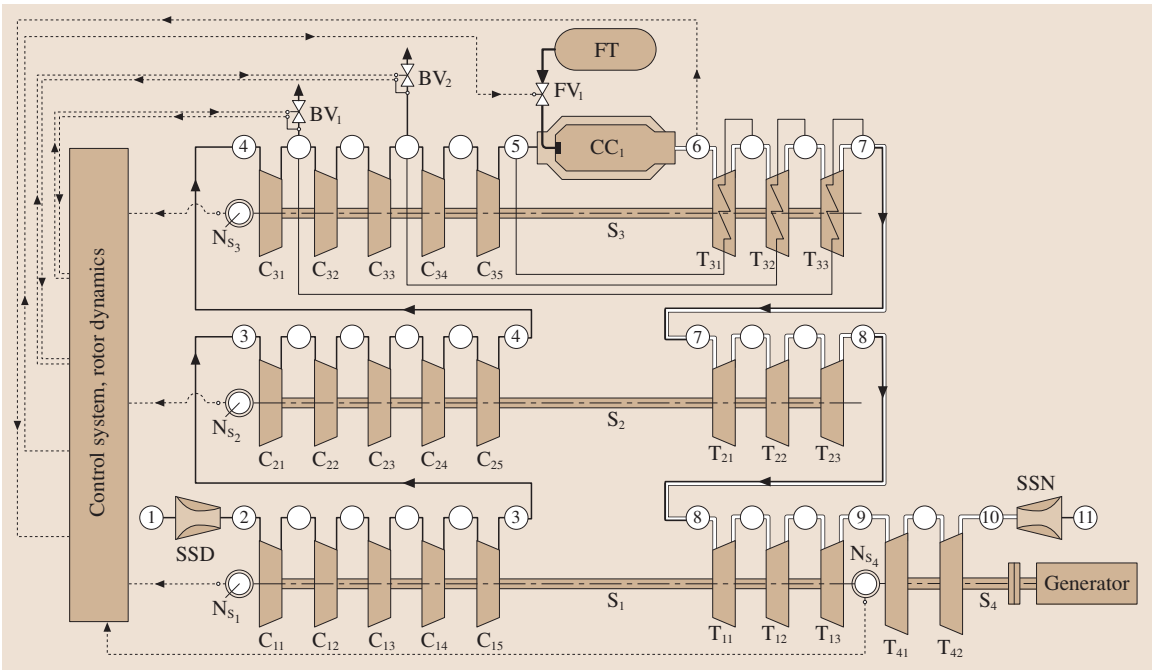


**Fig. 12.48** Simulation schematic of three-spool four-shaft high-performance gas turbine engine. Spool 1 incorporates the LP compressor and LP turbine connected via shaft $S_1$; spool 2 incorporates the IP compressor and IP turbine connected via shaft $S_2$; spool 3 incorporates the HP compressor and HP turbine connected via shaft $S_3$

The flame length extends from station 1 to 3, which makes segment number 2 the hottest one. As seen, the gas temperature at station 2 follows the sharp changes in the fuel schedule. By convecting downstream, these sharp changes are smoothed out. The wall temperatures shown in Fig. 12.52b exhibit similar tendencies.

*Compressor and Turbine Mass Flow Transients.* Figure 12.53a exhibits the compressor mass flow transients, which are dictated by the compressor dynamic operation. The difference in compressor mass flow is due to the mass flow extraction for cooling purposes. Turbine mass flows are illustrated in Fig. 12.53b. Except for a minor time lag, they show identical distributions. The

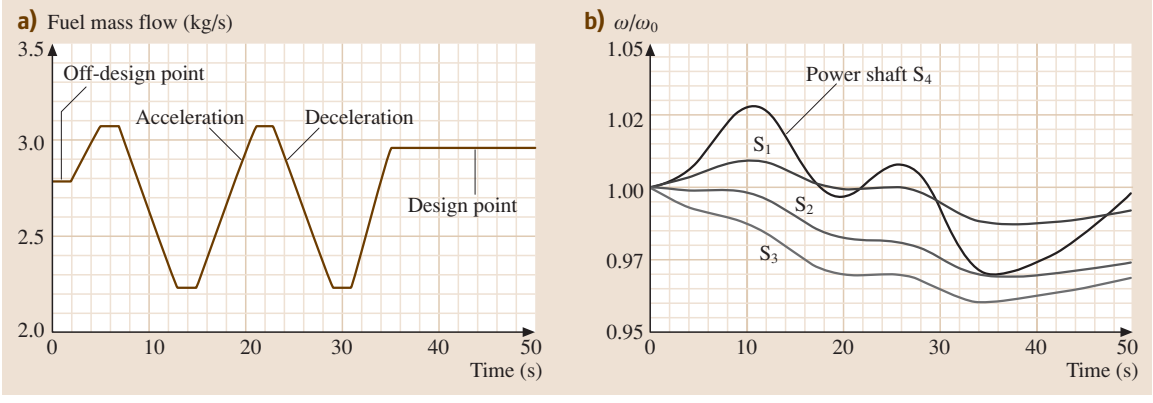


**Fig. 12.49** **(a)** Fuel schedule starts with an off-design mass flow followed by a cyclic acceleration–deceleration procedure. **(b)** Rotational speed of the three spools and the power shaft

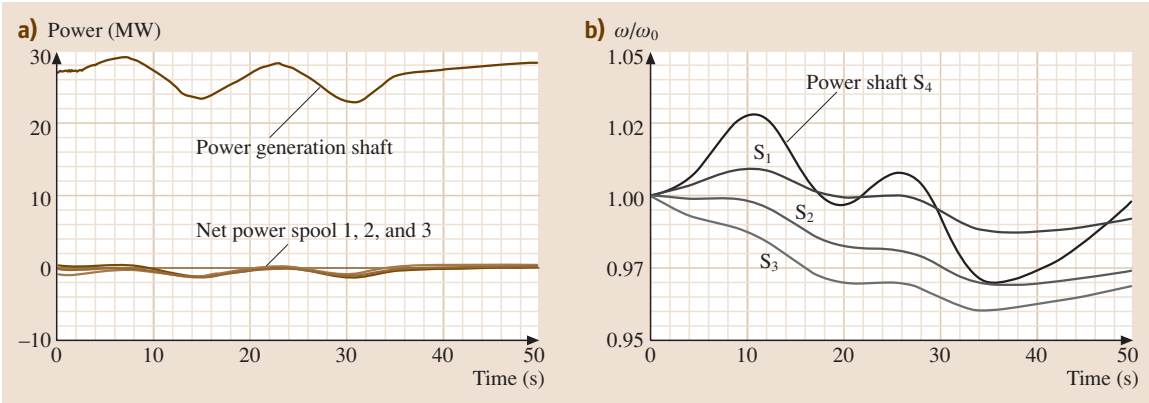


**Fig. 12.50** **(a)** Net power acting on the three spools causing a dynamic mismatch and the power generated by the fourth shaft. **(b)** Relative rotor speed of three spools and the fourth shaft

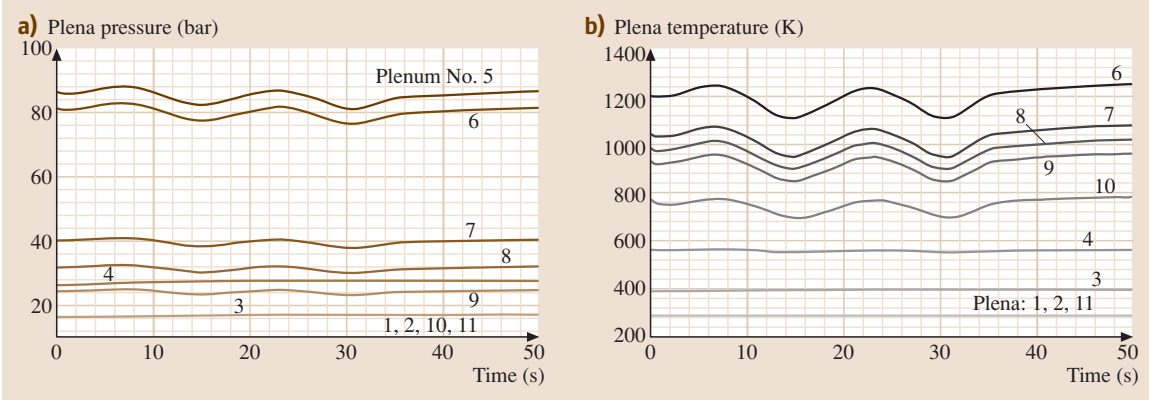


**Fig. 12.51** **(a)** Plena pressure and **(b)** temperature as functions of time

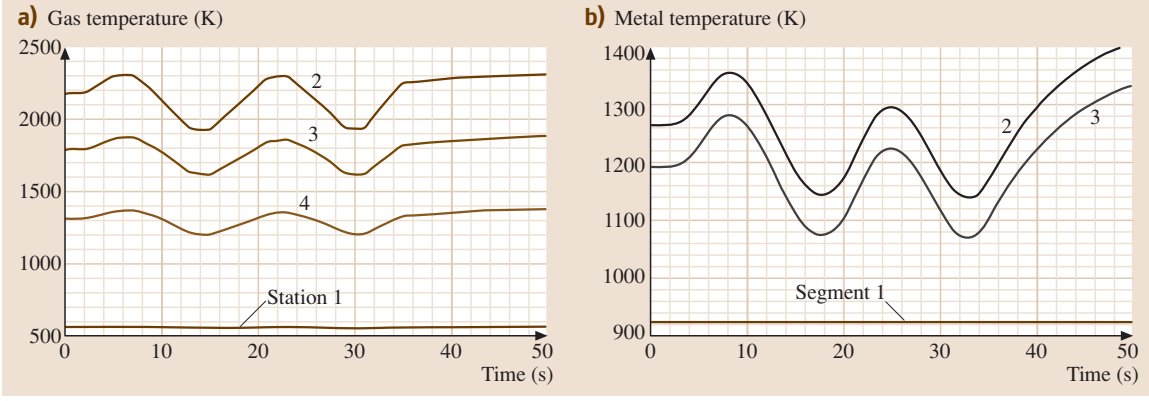


**Fig. 12.52** **(a)** Combustion chamber gas and **(b)** metal temperature as functions of time

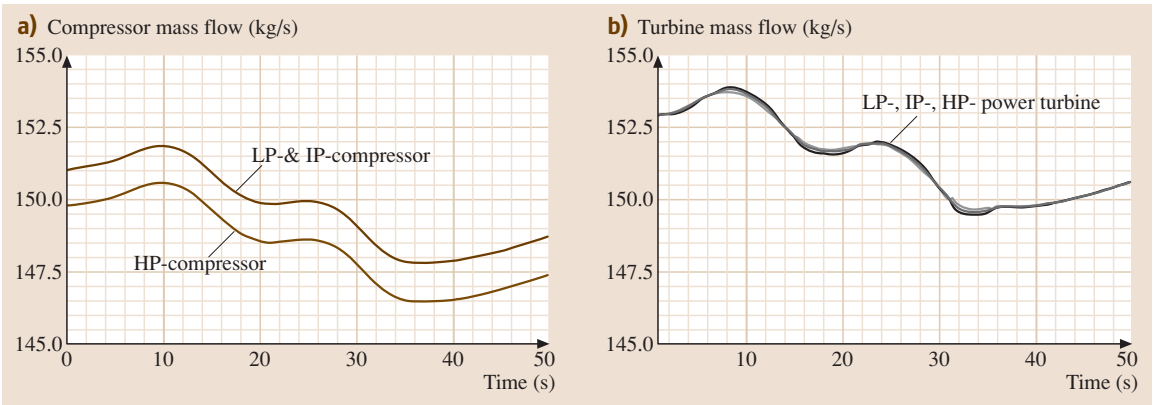


**Fig. 12.53** **(a)** Compressor and **(b)** turbine mass flow as functions of time

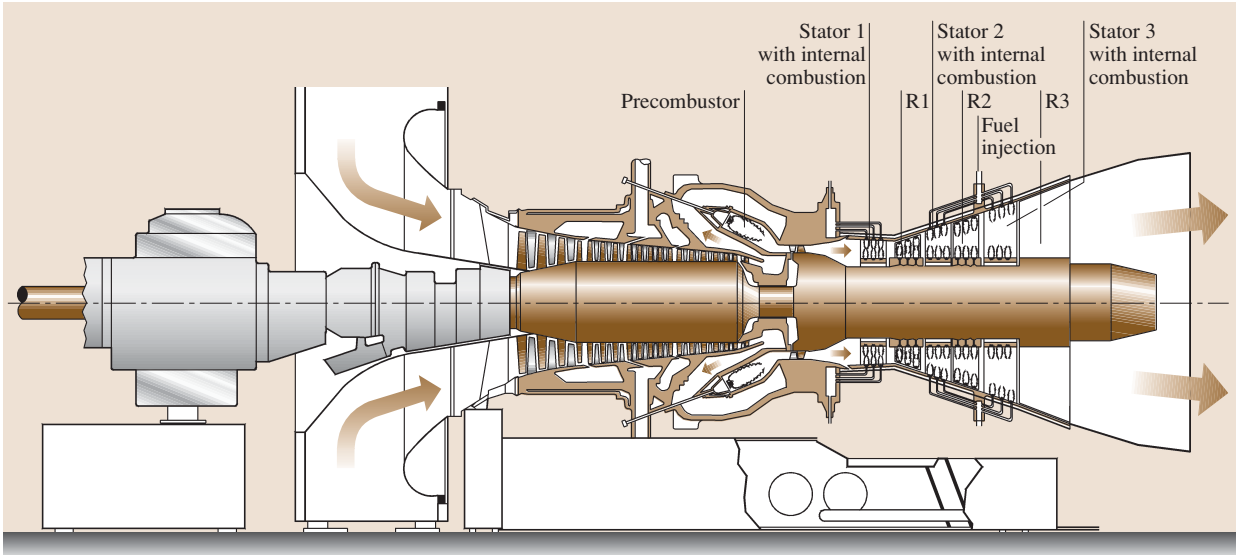


**Fig. 12.54** A derivative of the ultrahigh-efficiency gas turbine engine with a multistage compressor, a conventional combustion chamber PC, a single-stage reheat turbine RT, a three-stage turbine with an integrated stator internal combustion. B1, B2: compressor bypass blow-off, Fl1, Fl2: fuel lines to stator. The combustion process takes place inside the precombustor and stator flow path (after [12.7])

difference in turbine and compressor mass flow is due to the addition of fuel.

### 12.2.6 New Generation Gas Turbines, Detailed Efficiency Calculation

One of the interesting aspects of a dynamic simulation is the capability to calculate the gas turbine thermal efficiency dynamically during steady-state and dynamic operation. Such calculations are performed to compare the thermal efficiencies of four gas turbines with different design methodologies. The calculations are performed with the nonlinear dynamic code GETRAN©. The first gas turbine dynamically simulated for efficiency calculation is a conventional single-shaft, single-combustion chamber power generation gas turbine. The second one is the ABB GT 24/26. The third is an ultrahigh-efficiency gas turbine (UHEGT) with a precombustor, a reheat turbine stage, and an integrated stator internal combustion, as

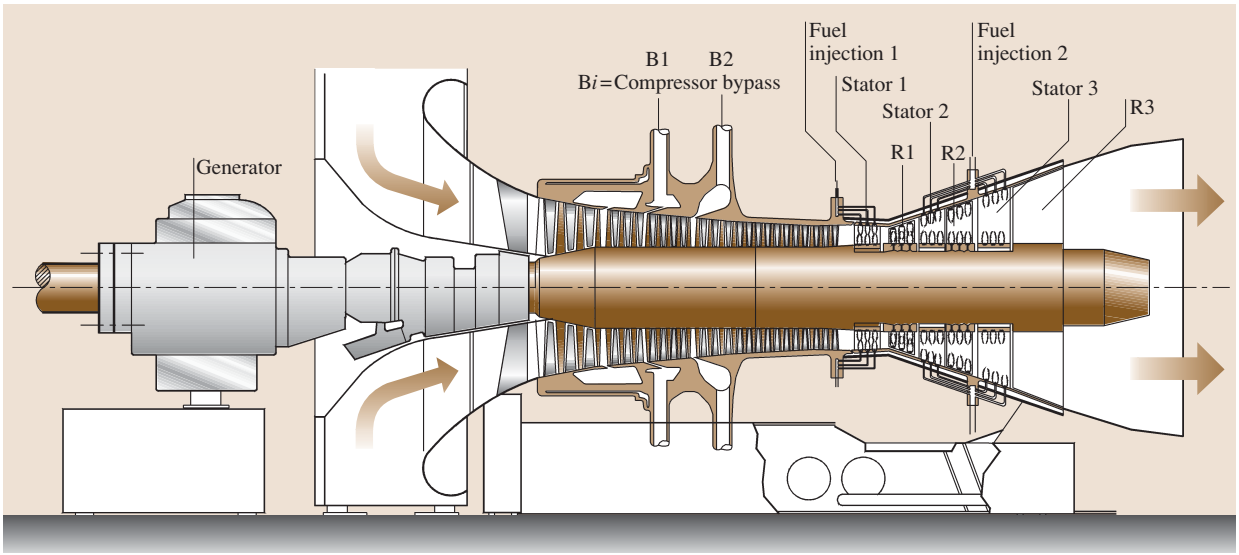


**Fig. 12.55** An ultrahigh-efficiency gas turbine engine with a multistage compressor, and a three-stage turbine with an integrated stator internal combustion. B1, B2: compressor bypass blow-off, Fl1, Fl2: fuel lines to stator. The combustion process takes place inside the stator flow path (after *Schobeiri* [12.7])

illustrated in Fig. 12.54. For the fourth gas turbine, the combustion process is placed entirely within the stator rows, thus eliminating the combustion chambers all together, Fig. 12.55. The dynamic efficiency calculation results are presented in Fig. 12.56. To accurately determine the thermal efficiency and specific work of the gas turbines, calculations are performed with GETRAN© and the results are presented in Fig. 12.56. To compare the degree of efficiency improvement, the thermal efficiency and specific work of a baseline GT, GT-24, and the three UHEGT gas turbines are included in the figures.

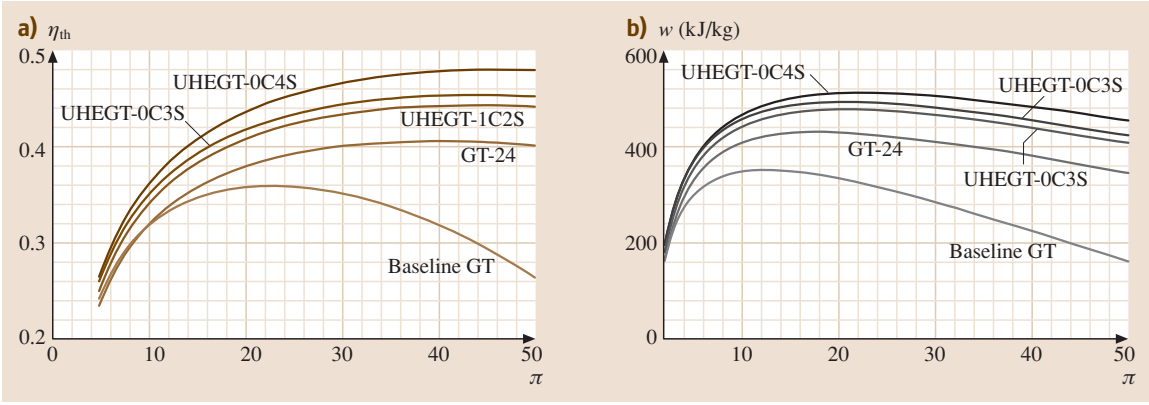


**Fig. 12.56** (a) Thermal efficiency and (b) specific work as functions of compressor pressure ratio for the reference baseline gas turbine engine, the ABB-GT-24 with two combustion chambers, the UHEGT-1C2S with one conventional combustion chamber and two UHEGT-stator combustion, the UHEGT-03S with three-stator combustion, and the UHEGT-0C4S with four-stator combustion. Turbine inlet temperature = 1200 °C, calculation with GETRAN (after [12.9])

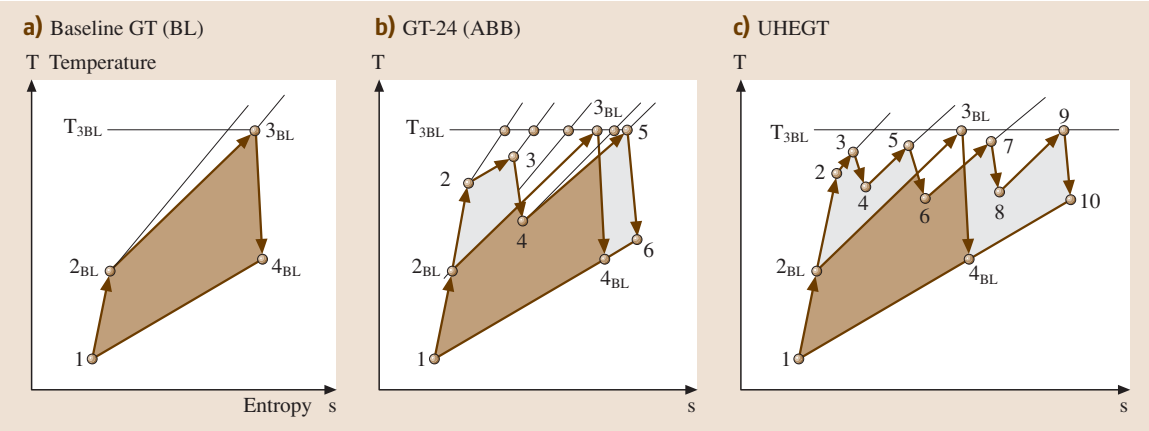


**Fig. 12.57a–c** Process comparison for (a) the baseline GT, (b) the GT-24, (c) the ultra high efficiency gas turbine technology (UHEGT) which has four stages with four integrated stator internal combustion

For a UHEGT with three-stator combustion, denoted by the curve UHEGT-0C3S, a thermal efficiency above 45% is calculated. This exhibits an increase of at least 5% above the gas turbine engine GT-24, which is close to 40.5%, as shown in Fig. 12.56a. Increasing the number of stators for internal combustion to four (curve labeled "UHEGT-0C4S") raises the efficiency above 48%. This is an enormous increase compared with any existing gas turbine engine. In the course of this calculation, the UHEGT technology is applied to a gas turbine engine with a precombustion chamber, such as the first one in GT-24 (Fig. 12.54). Using this combustion chamber with two-stator combustion, the curve labeled "UHEGT-1C2S" shows an efficiency of 44%. This is particularly interesting for upgrading the existing gas turbines with UHEGT technology. Figure 12.56b shows a comparison of the specific work for the gas turbines discussed above. Compared to the GT-24, UHEGT technology has about 20% higher specific work, making these engines very suitable for aircraft, stand-alone, as well as for combined cycle power generation applications. The evolution of the gas turbine efficiency improvement is summarized in the corresponding $T$–$s$-diagrams presented in Fig. 12.57a–c. In addition to the efficiency improvement brought about by utilizing a reheat turbine and two combustion chambers already discussed in conjunction with Fig. 12.26a,b further improvement is achieved by using stator internal combustion. As shown in Fig. 12.54c, with the UHEGT facilitates *quasi-Carnotising the Brayton cycle*. It is interesting to note that this efficiency increase can be established at a compressor pressure ratio of $\Pi_{\mathrm{UHEGT}} \approx 35\text{–}40$, which can be achieved easily by existing compressor design technology with high polytropic efficiency. In performing the GETRAN© calculation, compressor and turbine efficiencies are calculated on a row-by-row basis. This automatically accounts for an increase of secondary flow losses based on aspect ratio decrease. Thus, in a compressor case, efficiency decrease with pressure ratio increase is inherently accounted for.

## References


12.1 M.T. Schobeiri: *Turbomachinery Flow Physics and Dynamic Performance* (Springer, Berlin, Heidelberg 2004)

12.2 M.H. Vavra: *Aero-Thermodynamics and Flow in Turbomachines* (Wiley, New York 1960)

12.3 W. Traupel: *Thermische Turbomaschinen*, Vol. 1 (Springer, Berlin, Heidelberg 1977)

12.4 J.H. Horlock: *Axial Flow Compressors* (Butterworth, London 1966)

12.5 J.H. Horlock: *Axial Flow Turbine* (Butterworth, London 1966)

12.6 M.T. Schobeiri: Digital computer simulation of the dynamic operating behavior of gas turbines, J. Brown Boveri Rev. **74**(3) (1987)

12.7 M.T. Schobeiri: The ultra-high efficiency gas turbine engine with stator internal combustion, UHEGT Patent 1389-TEES-99 (1999)
12.8 M.T. Schobeiri, S. Attia: Advances in nonlinear dynamic engine simulation technology, ASME 96-GT-392, Int. Gas Turbine Aero-Engine Congress Exposition (Birmingham 1996)
12.9 M.T. Schobeiri, M. Abouelkheir, C. Lippke: GETRAN: A generic, modularly structured computer code for simulation of dynamic behavior of aero- and power generation gas turbine engines, ASME Trans. J. Gas Turbine Power **1**, 483–494 (1994)